Towards a data platform for multimodal 4D mechanics of material microstructures

Aldo Marano, Clément Ribart, Henry Proudhon

▶ **To cite this version:**

Aldo Marano, Clément Ribart, Henry Proudhon. Towards a data platform for multimodal 4D mechanics of material microstructures. Materials & Design, 2024, 246, pp.113306. 10.1016/j.matdes.2024.113306 . hal-04760746

HAL Id: hal-04760746
https://hal.science/hal-04760746v1

Submitted on 30 Oct 2024

HAL is a multi-disciplinary open access archive for the deposit and dissemination of scientific research documents, whether they are published or not. The documents may come from teaching and research institutions in France or abroad, or from public or private research centers.

L'archive ouverte pluridisciplinaire **HAL**, est destinée au dépôt et à la diffusion de documents scientifiques de niveau recherche, publiés ou non, émanant des établissements d'enseignement et de recherche français ou étrangers, des laboratoires publics ou privés.

Materials & Design 246 (2024) 113306

Contents lists available at ScienceDirect

Materials & Design

journal homepage: www.elsevier.com/locate/matdes

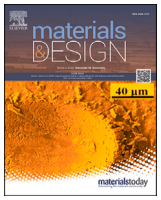

Towards a data platform for multimodal 4D mechanics of material microstructures

Aldo Marano [a], Clément Ribart [b], Henry Proudhon [b,*]

[a] DMAS, ONERA, Université Paris Saclay, F-92322 Châtillon, France
[b] MINES Paris, PSL University, MAT - Centre des matériaux, CNRS UMR 7633, BP 87, 91003 Evry, France

ARTICLE INFO

Keywords:
Data standards
Data management
4D experiments
Microstructure digital twins
Multimodal mechanics

ABSTRACT

This paper presents advances in the data management strategy applied to 4D multimodal mechanics of material sample microstructures. Guidelines to build a data platform allowing for complex workflows, involving several high-throughput experimental and numerical techniques, and complying with FAIR data management principles, are discussed. Next, their implementation within the open-source Python package Pymicro is presented, offering a high-level interface to build complex datasets through multimodal methodologies. Its capability to enable and automate complex workflows by building a digital twin of a commercially pure titanium sample under tension are then demonstrated. The digital twin contains microstructural and mechanical data for thousands of grains gathered on the same sample through synchrotron DCT and in-situ SEM experiments, as well as full-field numerical simulation. Finally, a local and statistical comparison between simulation and measurements of plastic slip and crystal rotation in hundreds of grains is shown, as an example of the contribution of this platform to multimodal data convergence and its importance for the development of a new generation of material models.

1. Introduction

Mechanical properties of structural polycrystalline materials result from the complex interplay of deformation and damage mechanisms with their internal microstructure. Thus, improving knowledge of microstructure-properties relation has long been a key issue for materials scientists, yet difficult because of the geometrical and physical complexity of the phenomena involved. Nowadays, automated and high-troughput microscopy and 4D imaging techniques, associated to large-scale simulations powered by high-performance computing (HPC) facilities [1], make it technically feasible to build multimodal datasets of unmatched richness to characterize and study these phenomena.

In-situ SEM experiments with many structural materials, involving digital image correlation (SEM-DIC) [2,3], high-resolution electron backscatter diffraction (HR-EBSD) [4,5] and/or electron channeling contrast imaging (ECCI) [6,7], have become a well established tool to characterize with sub-micron resolution deformation [8], damage [9–11], fatigue crack propagation [12–16] or intragranular plastic slip [17–23], and correlate their evolution with microstructural features. The very last advances in this field have made it possible to automatically analyze tens of thousands of plastic slip events [24–26], on regions that may reach several squared millimeters [27]. Although limited to the characterization of in-plane deformation of the observed surface, electron microscopy can be complemented by measurements using confocal microscopy to access the associated out-of-plane deformation [28,29].

Simultaneously, the blossoming of 3D microstructure characterization techniques during the two last decades has been a major step forward in the understanding of surface deformations, by providing the essential knowledge of the underlying microstructure and deformation state. Dual-beam focused ion beam–scanning electron microscope (FIB–SEM) allows to use electron microscopy to produce destructive 3D microstructural characterizations of polycrystalline samples with high resolutions [30–33]. On the other hand, techniques enabling to perform in-situ characterizations in 3D at the micro-scale have developed, building on the development of laboratory and synchrotron X-rays sources. Indeed, in-situ damage observation with X-ray computed tomography (X-CT) [34–38], characterization via X-Rays diffraction of polycrystalline materials microstructure [39–41] and deformation [42–44], and even 3D imaging of bulk plasticity [45], are becoming more and more efficient, automated and accessible [46].

As a result of the maturity now reached by these different tools, the last few years have seen the emergence of multimodal studies combining two or more of these [47] for the investigation of polycrystalline

* Corresponding author.
E-mail addresses: aldo.marano@onera.fr (A. Marano), henry.proudhon@minesparis.psl.eu (H. Proudhon).

https://doi.org/10.1016/j.matdes.2024.113306
Received 2 May 2024; Received in revised form 24 July 2024; Accepted 9 September 2024
Available online 11 September 2024
0264-1275/© 2024 The Authors. Published by Elsevier Ltd. This is an open access article under the CC BY license (http://creativecommons.org/licenses/by/4.0/).

materials mechanics. Very challenging, this approach culminates in the construction of large scale 3D multimodal datasets where microstructural and deformation measurements are well spatially aligned [48]. Such studies have notably focused on highlighting the complex deformation mechanics at triple junctions in polycrystals [49], the differences observed in slip transmission between surface and bulk grains [50], or the link between slip localization and intragranular orientation deviation statistics [51].

In parallel, advances in parallel computing, HPC facilities and digital 3D representation of both synthetic or real microstructures [52–55], supported the emergence of full-fields numerical models, based on the finite element method (FEM) [56–58] or on FFT-based solvers [59–62], for non-linear microstructure mechanics. Convergence of 3D computational models and characterizations opens up numerous perspectives, such as to study the influence of intrinsically three-dimensional microstructural features on the micromechanics of polycrystalline materials [63], or the possibility to identify micromechanical models for damage or plasticity by quantitatively comparing local predictions at microscopic scale to in-situ measurements [64,65]. Compared to classical identification methods based on macroscopic stress strain curves, this route should bring models closer to the micro scale physics of materials, by fully accounting for the evolution, geometrical complexity and microstructure dependence of these strongly non-linear phenomena [66,67]. On the other hand, simulation relying on trusted models can be used to enrich 4D experiments, by predicting quantities that cannot be measured [68–70], such as local heterogeneity of stresses and/or plasticity fields. It has been shown recently that these augmented datasets are well suited candidates to train machine learning algorithm to predict microstructure property relationship for complex processes such as fatigue short crack propagation [71]. Together with model order reduction approaches [72,73], they will extract value from these datasets to provide fast mechanical prediction tools enabling scientists to perform simulation driven 4D experiments, and accelerate the development of new materials.

As pointed out by a recent review [74], the aforementioned advances foster therefore the development of a multimodal approach of mechanical testing, combining for each sample the benefits of various characterization techniques and computational models. As constant increase of HPC power available and the arrival of 4th generation synchrotron sources will both contribute to significantly reduce simulation and testing time, data management appears to be one major obstacle towards the realization of this new paradigm. Indeed, it involves the gathering of very large amounts of data coming from many instruments, softwares, data formats, organized through long processing pipelines, whose technical complexity can become intractable. In addition, the expectations towards the use of machine learning algorithms in mechanics of material [75] is a further incentive to be able to assemble and automatically process large databases of such multimodal datasets. Therefore, the construction of unified data management infrastructures and standards enabling data interoperability, *i.e.* data platforms, is becoming a necessity.

Following recent efforts to build such tools for 3D microstructure characterization [53,76], this work proposes some guidelines to build a data platform able to relieve the technical burden specifically associated to multimodal and 4D methodologies to study material microstructures and their mechanical features. After a review of the technical challenges involved and of state-of-the-art data management tools among various scientific communities, a practical implementation of these guidelines, the open source Python package Pymicro, is introduced. Finally, an application to the multimodal study of the plasticity of a commercially pure titanium sample at grain scale, involving 3D microstructure characterization with synchrotron diffraction contrast tomography (DCT) of thousands of grains, SEM in-situ mechanical testing including EBSD scans, and intensive FFT-based crystal plasticity simulations. In particular, a detailed per grain comparison of the prediction of a crystal plasticity model from the literature and the measured lattice curvature is presented.

2. Data management strategies for multimodal material science

Management of large and multimodal data has been an issue for several decades now for some research communities, which have managed to build global data platforms that have significantly impacted their work. A short review of the key components of their success is provided here. An exhaustive review of platforms developed among all communities would go beyond the scope of the present paper. Rather, the focus is put here on a few mature platforms, widely used by their community. Specifically, it will be centered on astronomy and earth sciences, as they have long relied on multimodal imaging and large high-throughput instruments.

Astronomers have founded the International Virtual Observatory Alliance[1] (IVOA) to promote international use and interoperability of the colossal amount of observations delivered by an increasingly dense worldwide network of ground and space-based telescopes, operating at different resolutions and bandwidths. The concept of a virtual observatory (VO) embodies the vision that astronomical datasets must work together following the model of the World Wide Web: a single transparent system allowing astronomers to browse through all astronomical data. Hence, IVOA members work towards the development of standards allowing researchers to developed VO compatible tools instead of the unrealistic design of a monolithic tool fulfilling the needs of all users.

Their practical implementation has resulted in powerful and widely used astronomical data platforms, such as the ALADIN interactive sky atlas [77], providing online access to digitized images of the sky at various wavelengths, or the SIMBAD database [78] gathering physical features (object classification, coordinate, motion...) and observational data of millions of objects outside of the solar system, for decades of observations. Both are interoperable, which allows to use them to automatically query properties of objects in the database from images observed in the atlas, or the opposite, and send them to any VO compliant tool for processing. Another highly multimodal VO example is the Heliophysics Integrated Observatory[2] (HELIO) platform, is a European scientific infrastructure designed to support the needs of the Heliophysics community, overseeing data from more than 200 instruments (telescopes, probes...) observing the Sun. It provides a solar feature database generated by automated image processing codes from observations, that can be queried to find all data attached to a specific feature type for a specific time sequence and region of the Sun, and retrieved it in a VO compliant universal format. Similar organizations and platforms have emerged in the field of earth sciences, such as the Earth Observing System[3] or the Data TERRA[4] (EOS) initiative, that both coordinate the use of space, ground, and air-borne instruments to collect and integrate information about the Earth's land, atmosphere, oceans, and biosphere.

All these tools enable scientists to obtain and process relevant multimodal data on their objects of study from most advanced observation instruments, without technical obstacles. Among others, their functionalities include image, catalogue and spectra visualizations, statistical analysis, database queries. It is worth noting that these platforms operate at large scale, absorbing incoming data flows of several terabytes per day. In the following, the central elements of their success will be analyzed.

[1] https://ivoa.net/.
[2] https://www.helio-vo.eu/.
[3] https://eospso.nasa.gov/content/nasas-earth-observing-system-project-science-office.
[4] https://www.data-terra.org/.

2.1. Data standards

The first aspect common to the work of all these organizations has been the agreement on universal data standards. These have in common, notably, the definition of file formats (reviewed below), of specifications for table shaped data and lists of required metadata to describe data type and sources. They supervise in particular the possible content of datasets, as a collection of data item or data fields, defined at least by one name, a type and shape of data.[5]

A crucial part of their work for data and softwares interoperability point lies in specifications for representing spatially organized data, especially the arrays shape and ordering conventions. On this matter, important examples are the EOS specifications[6] to associate geolocation to scientific data, to organize and query data by earth coordinates and time, or the oceanographic measure format types specified by the SeaDataNet organization.[7]

Having well defined, agreed and documented standards has permitted the development of compatible and integrated softwares, dramatically simplifying all aspects of data access and processing for these communities.[8]

2.2. Scalable and hierarchical storage

In addition to data shape and format standards, these organizations have also settled on associated file formats. They all rely on file formats that are extensible, *i.e.* with no maximum size for the dataset, flexible and hierarchical. These two last features means that the format allows to gather multiple data items of virtually any type, size and dimensionality, and create links to organize them, building an internal file hierarchy similar to a file system, that closely corresponds to the application requirements. Together, these features allow to practically implement the data models defined in the data standards discussed in the previous paragraph. Two solutions stand out: raw data files encapsulated by a descriptive file (such as an XML file), or self-descriptive files.

The VOTable file format is an example for the first solution, that associates a FITS[9] binary file to an XML file describing its content. The second solution main examples are the popular NetCDF[10] and HDF5[11] formats. Both are open, portable, scalable and hierarchical binary files formats that allow in addition to include and manage metadata within the file itself. They have been developed together with open-source libraries providing simple and efficient interfaces for all major operating systems and programming languages, which helped their wide diffusion among scientists and industrials. In this way, NetCDF is one of the format agreed on by the SetDataNet organization, and have implemented their standard using the HDF5 format, creating the HDF-EOS[12] file format to support their data platforms. In addition, the HDF5 library supports many high-performance compression algorithms, which has proven to be a key asset to reduce the burden of the constantly increasing size of scientific datasets [46].

2.3. Computational integration and interfaces

To achieve a high level of computational integration between their data management services and expert tools, the aforementioned organization have followed a simple principle: building the data platform is about developing efficient interfaces between these tools. As a result, the platforms are designed with a *service oriented architecture*: each tool or service is developed as an independent software that however needs to comply with the data standards supporting the platforms, in order to facilitate communication between them. For this purpose, the IVOA has defined standardized protocols,[13] similar to web HTTP protocols, to exchange data between applications that follow their standards.

This architecture allows to build a platform whose services are not all geographically located at the same place. This allows, on the one hand, to distribute easily development and maintenance across the different organization stakeholders, and on the other hand, to increase the platform resilience. Indeed, if a service is unavailable at one location, it is very likely that its other instances can ensure the continuity of services. Moreover, this architecture ensures that the platform can be easily extended, as the implementation of a new service required only to comply with data standards and exchange protocols. The already mentioned HELIO and the bio-imaging BISQUE [79] data platforms are two large scale working examples of such architectures. They offer a complexity reduced to a minimum for users, to remotely access and chain numerical services thanks to GUI services of workflow managers. One last important element for tools integration that should be stressed is that these platforms are generally supplied with high-level Python APIs,[14] providing a simple access to the platforms services, and facilitating the development and integration of new tools for the platform.

2.4. State of the art for mechanics of materials

Some similar material science related initiatives have emerged in the past decade, such as the Integrated Computational Materials Engineering (ICME) [80] or the Material Genome Initiative[15] [81], that bolstered the development of several efficient platforms. Platforms such as AFLOW [82–84], the Material Project [85] or OPTIMaDe [86] provide tools and databases to link material compounds with their various physical properties. As they are based on established data standards, supported by Python APIs and integrated web platforms, they have become large scale infrastructures that gather millions of materials data.

In the field of microstructure mechanics, the structure of data itself is more involved because of the geometrical complexity of microstructure related data. The large body of work based on electron microscopy has led to the emergence of softwares for two-dimensional crystallographic data management, such as the MTEX Matlab toolbox, that fostered the development of interfaces between EBSD scans and various processing tools (visualization, meshing...)[16] More recently, Python libraries such as `orix`[17] also appeared to handle orientation data [87]. Initiatives such as the Nexus [88] format or the DREAM.3D environment [53] have developed data models and associated file formats to store and manipulate three dimensional microstructure descriptions. Notably, the format rely on the HDF5 file format. The DREAM.3D initiative has proposed to describe microstructures geometries through grids, through 3 levels of refinement: grid points, microstructure features (such as grains in polycrystals) and ensembles (such a phase in a multiphase materials). Its integrated and modular software environment has enable DREAM.3D to integrate several tools ranging from microstructure reconstruction, statistics, generation and meshing services, and to be integrated as a module within the web image processing platform BISQUE [89]. Recently, these efforts succeeded to link microstructure description tools

[5] see for instance the VOTable format definition https://www.ivoa.net/documents/VOTable/20191021/index.html.
[6] https://wiki.earthdata.nasa.gov/display/DAS/HDF-EOS+FAQ.
[7] https://archimer.ifremer.fr/doc/00454/56547/67033.pdf.
[8] see for instance the list of VO compatible toolshttps://ivoa.net/astronomers/applications.html.
[9] universal imaging data binary file format in astronomy.
[10] https://www.unidata.ucar.edu/software/netcdf/.
[11] https://www.hdfgroup.org/solutions/hdf5/.
[12] https://www.hdfeos.org/.
[13] see for instance the Table Access Protocol https://www.ivoa.net/documents/TAP/20190927/index.html.
[14] see for instance the HELIO platform Python API Sunpy https://sunpy.org/.
[15] https://www.mgi.gov.
[16] MTEX: https://mtex-toolbox.github.io/, MTEX based apps: https://mtex-toolbox.github.io/addons; see also Kanapy https://github.com/ICAMS/Kanapy or pyEBSD https://github.com/arthursn/pyebsd.
[17] https://github.com/pyxem/orix/.

Table 1
Pymicro Data Structures. Image, Mesh groups and Array (in bold face) are data structures dedicated to the representation of spatially organized data. All the rows contained between to solid lines belong to the same data group.

Pymicro Object	HDF5 Type	Description and Content	Metadata
Group	Group	standard group to organize data	Description text
Image	Group	group to store image-based data 2D or 3D regular grid Contains field arrays	Description text Dimensions Origin coordinates Grid spacing
Mesh	Group	group to store mesh-based data Nodes coordinates array Elements connectivity array Contains field arrays	Description text Dimensions Elements type list Elements sets list
Array	Array	standard N-dimensional array	Description text
Field	Array	Field values Array Nodal/Cell values Scalar, Vector, Tensor	Description text Type Dimensionality Time Parent Grid
Structured Table	Compound Datatype	Heterogeneous arrays: collection of sequences of named fields	Description text Fields names/types

to mechanical analysis, as illustrated by the recent PRISMS platform for microstructure-sensitive crystal plasticity [90] and fatigue [91] finite element analysis, whose microstructure data generation is supported by DREAM.3D or by the Neper software [52]. It is worth noting that Neper was recently more tightly linked with the FEPX software, dedicated to parallel finite-element crystal-plasticity simulation [92].

Yet, a more general approach designed to support multimodal workflows linking several imaging techniques at various dimensions and resolutions, fields measurements, microstructure statistics and numerical simulations, for several mechanical states of the same sample, is still lacking. As shown by this review, going down this path will necessarily go through the development and specification of data standards able to coordinate all these tools and softwares through simple and efficient interfaces. The rest of the present paper, is dedicated to the presentation of a data format, software package and multimodal study that aim to be a step towards this direction.

3. The Pymicro multimodal data management package

The Pymicro package is a Python library designed to work with material microstructures data, with a particular focus on polycrystalline materials. Pymicro's data module is structured around a file format and a generic data model, that are able to handle multimodal microstructure datasets, and are sufficiently flexible to be used to define and implement data standards. The package implements a high-level interface to create, access and manipulate datasets complying with this format, with a strongly reduced technical complexity for users. This interface also allows to quickly build interfaces with external numerical tools to simplify and automate data generation and processing. As such, it can be viewed as a data management service prototype that could support a multimodal 4D mechanics data platform. It is an open-source package, available and documented online.[18]

3.1. File format

Inline with the strategic choices reviewed above, Pymicro's data module is based on the HDF5 file format, an open, hierarchical and scalable format. In addition, companion XDMF description file (a XML based standard format for HPC applications[19]) may be generated for compatibility with the widely used 3D data visualization open-source software Paraview. On the other hand, efficient solutions exist nowadays to browse and visualize the content of very large HDF5 files, such as the Vitables[20] or Silx-view[21] softwares. Finally, the HDF5 library provides powerful compression algorithms, that are an essential asset for the management and storage of massive data.[22]

3.2. Data model

3.2.1. Data structures

As with the HDF-EOS format, Pymicro implements a data model that is a specification of the HDF5 data model, designed to map data structures with the various types of data used to characterize material samples. It is built from basic objects of the HDF5 format (groups, arrays, attributes), enriched by a specific set of metadata. The specification of the provided structures is indicated in Table 1. Each item in the dataset may be enriched with an arbitrary set of key/value pair metadata, using HDF5 attributes. In particular, the data model includes a description text metadata for each data item.

Spatially organized data, *i.e.* two or three dimensional field measurements, are key for modern material datasets sets. They are sets of values known at specific locations of a grid of points/cells. In line with the XDMF data model (adopted by the DREAM.3D software [53]), such data is represented by associating arrays describing the grid topology and the values of the field. The ordering of the latter are used to map field values to the appropriate grid point/cell. Two types of grids are distinguished: regular grids (images) and unstructured grids (meshes); As a grid is a container for fields, specifications of HDF5 Groups have been implemented to represent images and meshes. The metadata attached to these groups specify the topology and spatial location of the grid, and list the stored fields. Similarly, two types of fields are considered: nodal value and cell value fields. A specification of HDF5 data array is implemented to represent them, that has metadata specifying the nature of the field and its parent grid. The Image Groups and Mesh Group in Fig. 1 show a graphic illustration of such data structures.

Structured tables are another fundamental data structure. They are arrays with heterogeneous column types, *i.e.* a collection of records of values (rows) for a set of named fields (columns).[23] These are typically

[18] Github page: https://github.com/heprom/pymicro. Documentation: http://pymicro.readthedocs.io/.
[19] https://www.xdmf.org/index.php/Main_Page .
[20] https://vitables.org/.
[21] https://www.silx.org/doc/silx/latest/.
[22] Pymicro relies on the Pytables interface with HDF5 library and its compression algorithms http://www.pytables.org/.
[23] See Numpy structured arrays https://numpy.org/doc/stable/user/basics.rec.html.

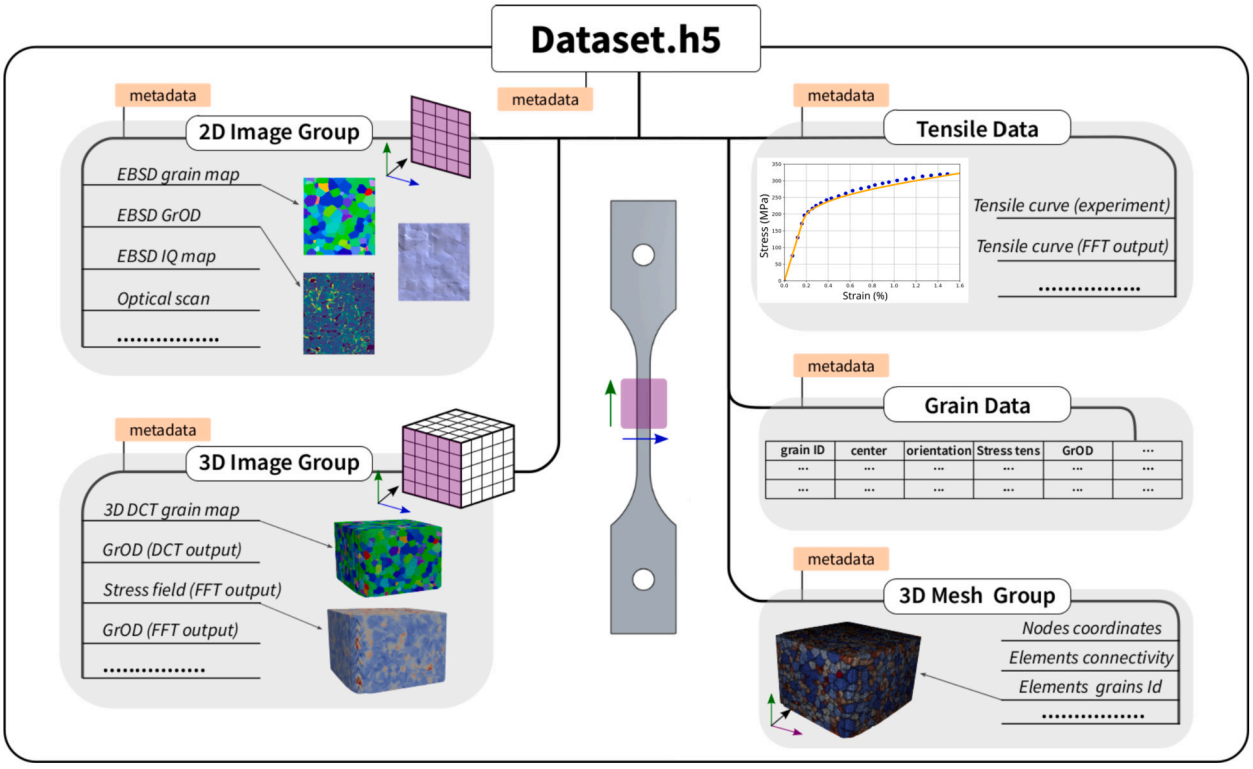

Fig. 1. Schematic representation the Pymicro dataset for the pure α-phase grade 2 titanium sample presented in section 4. The dataset conforms to the data model introduced in 2. Groups are represented by grey boxes. Groups marked with the grid icons have their data geometrically aligned with the sample frame. Regions in purple surfaces are geometrically aligned and correspond to the sample surface area highlighted in purple. Grains are identified by a grain identification number, mapped by "grain map" fields, and have been matched between the EBSD and DCT maps. This number is used in the grain data table to indicate which grain each row of data refers to, and in the mesh to identify the elements sets associated with each grain, for the sake of brevity, groups containing data relative to the α-phase properties is not represented.

used in Pymicro to describe the properties of a set of similar microstructure objects, such as crystallographic grains but it could also be used to describe other features such as defects in a material sample for instance. They can be represented by arrays using the HDF5 compound data types. Pymicro leverages the implementation of this mechanisms in the Pytables package, to offer a flexible interface with structured tables in datasets. The Grain Data group content in Fig. 1 show a graphic illustration of a structured table.

Finally, 4D experiments involve the description of the temporal evolution of a physical phenomenon. Standard arrays or structured tables can easily be leveraged to store time series of uni-dimensional, as illustrated by the Tensile Data group in Fig. 1. Conversely, time series of data maps are delicate to handle. Indeed, the physical grid used in the measurements or simulations may evolve in time. For instance, during a tensile test monitored by DIC, the material points move and change position in the pixel grid of captured images. These data can align on the same grid, using various registration processes. This is also readily the case for output fields of a simulation. In that case, the data model allows to input several values of a same field associated to several time values, within the same grid. They are then automatically stored as different arrays with a time value metadata, that can be used to identify, process or retrieve them. Pymicro also ensures their time encoding in XDMF format, which can be used to visualize the evolution of fields in animation with compatible software, such as Paraview. If the grids associated to each time are not aligned, then they may be stored, along with the data fields, in separate data groups. In both cases, data are tagged with a time description metadata.

3.2.2. *Polycrystalline microstructure data model*

An application-specific data model can be built by specifying an architecture composed with the data structures detailed in 3.2.1. Pymicro provides the means to implement such a data model in the form of a Python class derived from the generic dataset management. To implement it, the main task for users is to define the data model through simple Python dictionaries. Then, it can be leveraged to easily implement an application-specific high-level interface between users and datasets. Pymicro ensures that datasets handled by this new class conform to the prescribed data model, but does not restrict the possibility of enriching datasets with supplementary data.

This feature has been implemented for polycrystalline microstructures. As discussed in the introduction, image-based techniques are central for the characterization of these materials. Moreover, the overwhelming majority of works focus on grains as the elementary micromechanical entity to describe their behavior on a mesoscopic scale. Making the most of multimodal datasets thus implies being able to correlate different measurements/simulations at precise locations, or within precise grains of the microstructure. For this, the data must be aligned on the same image, and the grain/phase representation must be consistent with it.

The data model has been designed accordingly. Its main item is a reference image used to describe the microstructure and store all fields that have been geometrically aligned. This image contains three maps to describe the microstructure: a mask indicating regions with non relevant data, a map of phases, a map of grains. Two distinct phases differ in crystallographic structure and/or composition, while grains differ only from crystallographic orientation. These maps associate a unique identification number to each region corresponding to a distinct grain/phase. The grain map is then associated to a structured table to store per-grain data. The synchronization between the maps and the table is ensured by the class using the identification number. The data model includes additional items to store mesh-based data, and the description of the material phases. The data model is detailed on Table 2. It has been ex-

Table 2
Data Model implemented in Pymicro for polycrystalline microstructures. The type of data structure associated to each item is indicated in italics between brackets. The metadata associated to each data structure is indicated in Table 1 and is not reproduced here.

Polycrystalline Microstructure Dataset	
|– CellData	Reference microstructure image (*Image Group* - 2D or 3D)
|– GrainMap	Map of grains identification numbers (*Field* - integers)
|– PhaseMap	Map of phase identification numbers (*Field* - integers)
|– Mask	Map of relevant data in image (*Field*)
| – …	Any additional field geometrically aligned with the microstructure description (*Field* - binary): orientation map, DIC measurement, spectral solver simulation result...
|– LengthUnit	unit of length of data, usually µm (*Metadata*)
|– **MeshData**	**Microstructure mesh** (*Mesh Group* - 2D or 3D)
|– GrainIds	Element-wise field indicating correspondence between grains and elements (*Field* - integers)
| – …	Any additional node or element-wise field defined on the microstructure mesh (*Field*): finite element simulation results, FEM based DIC...
|– **GrainData**	**Description of microstructure grain properties** (*Group*)
|– GrainDataTable	Grains feature table (*Structured Table*)
	- grains Id number, center, volume, bounding box, crystal orientation
	- any additional per grain data (mean stress/strain tensor, reference orientation deviation, sphericity...)
|– **PhaseData**	**Description of microstructure phases** (*Group*)
|– Phase_1	Phase 1 description data (*Group*)
|– ElasticConstants	Elastic moduli of the crystalline phase (*Metadata*)
|– StressUnit	unit of stress for elastic moduli, usually MPa (*Metadata*)
|– LatticeSymmetry	Symmetry of the crystalline phase (*Metadata*)
|– LatticeParameters	Crystal lattice parameters of the phase (*Metadata*)
|– LatticeLengthUnit	unit of length for lattice parameters, usually nm (*Metadata*)
|– Formula	Chemical Formula (*Metadata*)
| – …	…
|– Phase_*i*	Phase *i* description data (*Group*)
| – …	…
| – …	Additional Images, Meshes, data Groups... (*Group*)
| – …	additional arrays, fields, metadata, structured tables...

plicitly adopted within Pymicro, and generalized to the storage of all types of data according to this hierarchy. Note that this is a minimal, non-rigid data model: as much additional data as desired may be stored and manage by the interface.

Fig. 1 provides a complete example of a dataset assembled with Pymicro and conforming to the aforementioned data model. The data comes from various characterization and simulation techniques, detailed in section 4. The dataset microstructure reference image is the 3D Image Group. Using the Pymicro interface, an additional two dimensional image has been geometrically aligned with a specific surface of the volume. The grain data table, in the Grain Data group, is used to store the average value for each grain of some fields, such as crystal orientation, topology, phase, stress state, …), using a separate line for each grain. The dataset also contains a mesh with element sets that are associated to each grain, via the same grain identification number; and a standard Group, Tensile Data, to store the time series of stress/strain measurements of a tensile test. Each metadata node may contain an arbitrary number of user defined supplementary Attributes.

3.3. Interface

The Pymicro data management module provides a Python API to interact with datasets. It offers methods to cover all generic data management tasks: create, remove, modify and organize datasets, data items of all types and metadata, access and visualize dataset content and data item values, but also manage individually compression settings of each data item. Each method implements an independent data management task, with an explicit name and simple interface. Hence, they can be seen as modular elements that can be assembled to create a processing pipeline.

The base layer of the package is the *SampleData* class, that implements the core dataset management functionalities and the base data structures. It also provides a generic interface to create and assemble datasets

This class is design to be used to derive classes with an application specific data model, simply declared via Python dictionaries indicating the data model architecture and data structure types. In this way, the data model presented in Table 2 has been implemented via the *Microstructure* class. It is designed to be a high-level interface for end users that collect and process the data for scientific purposes. It ensures that created dataset automatically conform to the microstructure data model, and provides visualization, management and processing tools that are optimized for the data structure and the needs of polycrystal mechanics. The capabilities of this interface is highlighted in section 4 and can be appreciated from the online resources [93–95] that have been used to produce the results of section 4.5. This allows simultaneously to showcase the capabilities and to reproduce the results obtained via EBSD, DCT characterization and CP-FFT analysis.

These examples illustrate how Pymicro lets a end-user interact with datasets. For the sake of brevity, the interface will not be detailed further in the present paper. A detailed description is available on the package documentation website.

3.4. Integration with external tools

The interface simplicity has been leveraged to extend the API to automate interaction with several numerical tools. These modules handle the technical aspects of data exchange and formatting, and may also run the external tool as a master application, enabling automated interac-

tion with datasets from the Pymicro interface. They include interfaces with:

- the finite element analysis suite Zset [96];
- the FFT based homogenization solver AMITEX_FFTP[24];
- the output format of the microstructure data management and generation softwares DREAM.3D [53] and Neper [97];
- the output formats of the EBSD microstructure generated by EDAX and Oxford instruments;
- the output format of the DCT reconstruction Matlab based program developed at ID11[25];
- the output format of GrainMapper software commercialized by XNovoTechnology[26] for laboratory based DCT reconstructions [98];
- an multi-phase image meshing software [99].

Users can then implement complex data processing workflow involving all of these tools, directly from the Pymicro dataset interface, without requiring expert knowledge of the all the data formatting requirements involved. A practical example is provided in the next section.

4. Application: multimodal investigation of the mechanical behavior of a polycrystalline material

The Pymicro package played a important role in facilitating a comprehensive investigation into the micro plasticity involving several imaging modalities of a commercially pure α-phase grade 2 titanium (CP-Ti family) specimen. This study aimed to achieve three critical goals: first, the acquisition of a 3D representation of the microstructure; second, the conduction of in situ measurements capturing grain-scale plasticity dynamics during a controlled tensile test; and third, a rigorous comparison of these experimental observations against the predictions derived from a microstructure-sensitive crystal plasticity simulation. This simulation was conducted on a digital twin of the titanium sample, aiming to assess the predictive accuracy of the model at the local scale.

4.1. Samples preparation

The studied material was a TIMET cold-rolled sheet, measuring 1.6 mm in thickness with an homogeneous microstructure characterized by equiaxed grains with an average size of 15 μm. Preliminary electron backscatter diffraction (EBSD) characterization revealed the presence of a pronounced texture that is characteristic of hexagonal close-packed (HCP) rolled sheets, as described in [100]. To reduce the number of grains in the cross section and comply with DCT requirements, a heat treatment was employed to foster grain growth, resulting in an average grain size of 37 μm. This thermal cycle spanned 24 hours, maintaining a temperature plateau of 855 °C, just below the β-transus point, and utilizing a continuous flow of argon at a rate of 10 L/min. The treated sample was subsequently quenched using air cooling. Specimens with a dog-bone geometry and a 600 μm wide square gauge section (see Fig. 1) were machined along the rolling direction (RD) using electron discharge machining (EDM). To eliminate any surface irregularities and any residual stresses introduced during the machining process, all four faces within the central region underwent pre-polishing using 1,200-grit silicon carbide paper. This step helps to achieve optimal diffraction performance for DCT acquisition even close to the specimen surface. In addition, one face was further polished with 2,400 and 4,000 grit sandpaper followed by a 30 h mechano-chemical polishing using a 50% water with 50% 60 nm colloidal EPOSIL M silica solution. To enable precise tracking of strain load during subsequent tensile testing, fiducial micro-indents were strategically placed at the center of this face, delineating a well-defined domain of interest. At this point, a reference EBSD scan was conducted to capture the initial microstructure of the sample's surface prior any deformation.

The authors would like to emphasize that despite a rigorous preparation and a mirror finish with EBSD quality, the surface polishing turned out not totally optimal. One can notice the presence of a parasitic speckle – observed as dark regions in the middle of the grains – depicted in the EBSD Index Quality (IQ) map shown in Fig. 3.b.ii. With such a small specimen geometry, and despite several attempts and techniques tried (electropolishing, mechanical polishing, ion-beam polishing), this could not be avoided. Such difficulties were not experienced on larger surfaces. As detailed later in section 4.5.2, this pattern prevents diffraction locally and disturbs the orientation field in its vicinity. Insight from atomic force microscopy (AFM) has provided indications that these speckles correspond to nanometric-sized recesses, penetrating to a depth of approximately 15 nm. Subsequently, to avoid accounting for these regions, the EBSD data was processed with a stringent segmentation in Pymicro (no cleaning, minimum tolerance angle set to 0.7° and 150 pixels minimum grain size) to exclude the parasitic zones and process only reliable data points. A clean grain map was further achieved via dilation but only for visualization purpose.

As a last note on the initial microstructure observation, the presence of a non diffracting micron-sized lamellar precipitates at grain boundaries was detected by secondary imaging (SE) SEM observations, mostly at triple junctions. This precipitation originates from the heat treatment which allowed diffusion of Fe, followed by a precipitation during quench. These regions are the only non diffracting regions in the EBSD. Away from triple junctions, the signal diffracts well (apart from the aforementioned parasitic speckle issue), even at grain boundaries.

4.2. Experimental procedures

4.2.1. Reference diffraction contrast tomography scan

First, a reference Diffraction Contrast Tomography (DCT) scan was performed prior to the EBSD in situ test. This allowed to capture the underlying 3D crystallography map of the real microstructure. The synchrotron DCT technique, developed at the ESRF [101] is a monochromatic near-field variant of 3D X-ray diffraction (3DXRD) [102] using a box beam illumination and collecting images spanning a full 360° rotation in order to reconstruct the polycrystalline microstructure morphology with the crystallographic orientation in each grain. As such it can be considered as a 3D non destructive EBSD. The sample was scanned at the ESRF ID11 beamline after the EBS upgrade. The beam energy was set to 43.5 keV. The detector used was an ANDOR Marana sCMOS camera with a 2,048×2,048 pixels array, resolution set at 1.22 μm and positioned 6.5 mm downstream from the sample. The illuminated region of the specimen spanned a height of 407 μm and the scanning process took 3 minutes.

4.2.2. EBSD interrupted in situ experiment

Some of the prepared samples were used for preliminary laboratory tensile tests under optical microscopy, yielding macroscopic stress-strain curves (see Fig. 2.d). For the in situ experiments, the FEI Nova NanoSEM 450 at the Centre des Matériaux, coupled with a Newtec MT1000 test-rig and EDAX OIM Hikari EBSD camera, was utilized. After tilting the cradle to 70°, a 1.5-hour, undeformed EBSD map (730 μm × 410 μm) was acquired at ×130 magnification, with a voltage of 20 kV, a current spot of 5 nA, a step size of 1 μm, a camera binning of 2, all resulting in an approximate angular resolution of 0.5°. Sequential EBSD scans at 0.6%, 0.9%, and 1.6% deformation were executed under consistent conditions after repositioning the sample to cover the same area. All scans were conducted partially unloaded to prevent potential relaxation and cold creep effects. Eventually, a post-mortem characterization of

[24] http://www.maisondelasimulation.fr/projects/amitex/general/_build/html/index.html.
[25] https://gitlab.esrf.fr/graintracking/dct.
[26] https://xnovotech.com/.

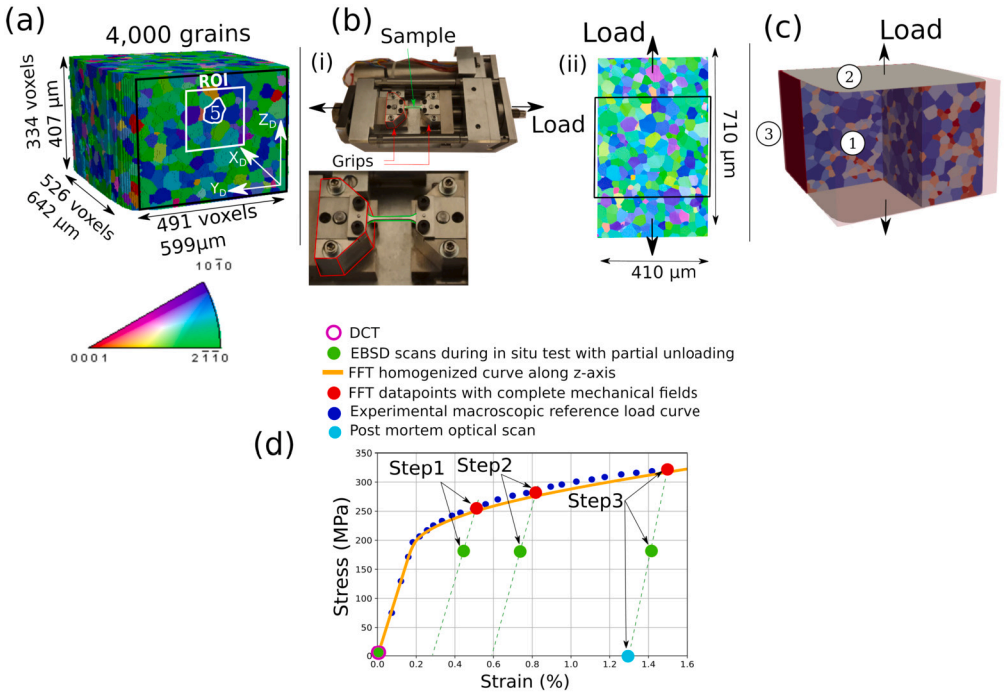

Fig. 2. In situ multimodal acquired data: a) Digital twin obtained from the DCT scan at ESRF ID11 after EBS upgrade with IPF-Z coloring with data written in the DCT reference frame (X_D, Y_D, Z_D). The white frame around the highlighted grain denoted *5* corresponds to the region of interest (ROI) studied later in section 4.5.3, b.i) In situ EBSD test rig with specific grips for DCT geometry specimens, b.ii) Final load step EBSD scan written in the same reference frame than the DCT data. The black frame on a. and b.ii highlights the common surface between the DCT and the EBSD data. c) FFT simulation setup with boundary condition: (1) denotes the material zone associated to the actual CP-Ti microstructure (except the precipitates), (2) denotes the grips, (3) represents void voxels around free surface, d) Stress-strain macroscopic load curve along z-axis. The large dots highlight where the different experimental characterizations were carried out.

the surface by optical microscopy with a LEICA DMI 5000, allowed to capture out of plane plastic slip activity in the form of slip bands. The different acquisition data points are highlighted in Fig. 2.d.

4.3. Digital twin reconstruction and dataset instantiation

A 3D digital twin of the DCT scan was reconstructed using the ESRF program developed by the team at the Materials Science beamline ID11[27] [101,103,104]. With the 3D-DCT approach tailored for non-deformed microstructures, a raw volume containing 4,000 grains, each with a single orientation, was generated. A first cleaning step (mainly to merge grains that were reconstructed twice) was performed using an assistant within the DCT program. A few missing grains, 13 in this case, located on the lateral faces were also added manually with random orientations. Pymicro provided additional numerical cleaning and grain dilation functions to obtain a refined grain map suitable for simulation. Complementary PCT measurement can be performed, first to provide a high resolution mask for the reconstruction of the DCT volume, second to capture the presence of the lamellar beta phase. Indeed, if the sample-to-detector distance is sufficient (150 mm here) this phase becomes visible and can be reconstructed. In the scope of this paper, the focus was drawn to reconstructing a large (several thousand grains strong) polycrystalline microstructure and the beta phase was not investigated (the PCT scan was performed at a 30 mm distance).

The Pymicro microstructure dataset was instantiated from this reconstruction. Identifying common areas among modalities was achieved by taking advantage of the fiducial indents and IPF color coding of orientation maps. Ensuring a shared reference frame between EBSD and DCT modalities greatly facilitated direct comparison. Integration of all modalities into the Pymicro dataset was executed seamlessly using platform-provided commands. Note that here, comparisons are carried out at the grain level (e.g. grain orientations, slip system activation, misorientation level, etc). Since each modality has its own reference frame, finding the same grains in the different modalities is not straightforward. By expressing orientation data in a common reference frame (both for orientation data and for the spatial representation of the data), a grain matching algorithm can be used. Here a simple algorithm based on the closest orientation was used to match grains between EBSD and DCT modalities. Additionally, Pymicro offer the possibility to register one data set with respect to a reference data set (this can be used for instance to correct distortions in EBSD acquisitions). Using this method would allow to carry out comparison at the pixel/voxel level as demonstrated in [105].

4.4. Numerical simulation

A numerical simulation was carried out on the 3D microstructure image reconstructed from the DCT experiment, using the FFT-based full field mechanical solver AMITEX_FFTP.[28] For details on the numerical implementation, the reader is referred to previous work [106]. The simulation employed the finite strain viscoplastic crystal plasticity model developed by Marchenko et al. [107] for CP-Ti grade 2. It has been carried out on the Jean Zay CNRS supercomputer, using 1000 cores. In these conditions, the simulation took about 40 minutes to complete. This formulation encompasses basal, prismatic and type-I pyramidal slip systems and does not include strain aging effects. To account for the slightly lower concentration of oxygen compared to the batch studied by Markencho, Doquet and Barkia, the critical resolved shear stresses of the different families were lower down by 10%. Indeed, higher oxygen interstitial concentration increases the yield stress for CP-Ti as reported in [108]. The simulation was conducted with boundary conditions replicating the in situ SEM test conditions (see Fig. 2.c). The simulation

[27] https://gitlab.esrf.fr/graintracking/dct.

[28] https://amitexfftp.github.io/AMITEX/index.html.

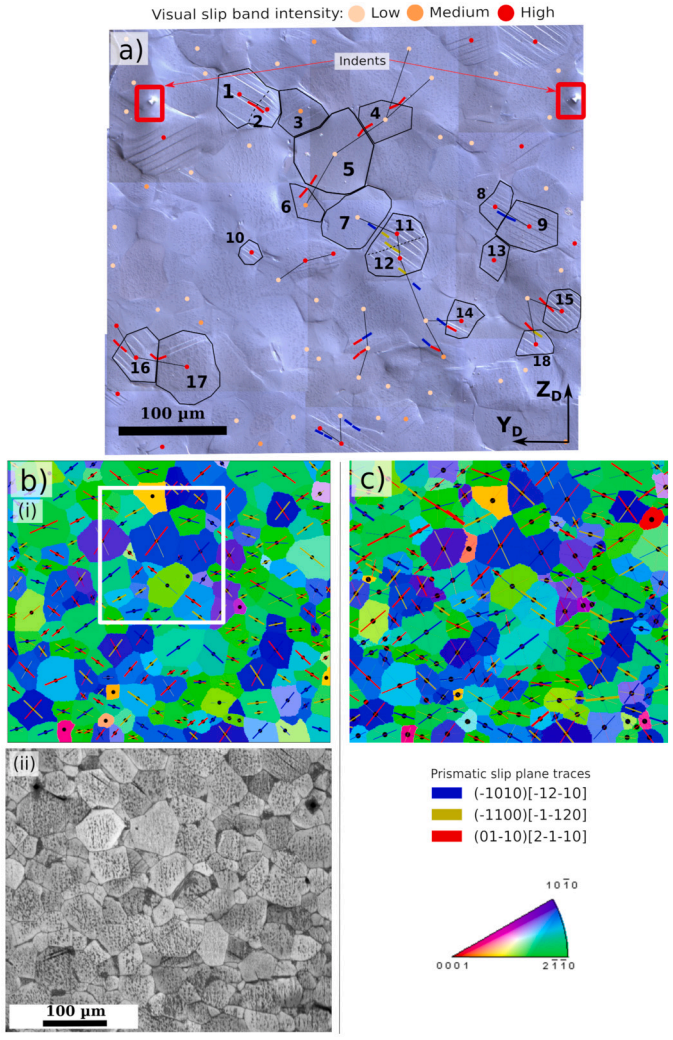

Fig. 3. Multimodal slip activity analysis over the full height of the digital twin on the EBSD face at final load: a) Post Mortem optical stitched map with slip bands visible at the free surface. Fiducial indents are highlighted as they can locally affect the plastic activity, b) EBSD data: (i) OIM map with IPF-Z coloring after numerical cleanup. The map is overlaid with prismatic slip plane traces with colors as per arbitrary convention from Table 3. The lines thickness is proportional to the Schmid Factor for the corresponding slip system. The white frame reminds about the region of interest (*ROI*) studied later in section 4.5.3, (ii) OIM IQ map, c) FFT data: Pymicro map of the DCT digital twin restricted to the EBSD face. Similarly to b.i, the map is overlaid with prismatic slip plane traces. This time the lines thickness corresponds to average activity per grain for each prismatic system. Differences in IPF coloring between the OIM and the Pymicro maps are due to default display differences.

incorporated layers with null elastic coefficients surrounding the sample, to impose traction-free conditions on the sample's lateral surfaces. Additionally, a stiff elastic layer buffer has been added along the tensile direction, in order to mitigate the influence of the periodicity imposed by FFT-based solvers, on the grains cut by the surfaces normal to that direction. The simulation input data has been automatically generated with Pymicro from the 3D microstructure description stored in the dataset. The tensile test simulation matched the in situ deformation level, and provided the mechanical fields of the elastic strain and lattice rotation tensor, Cauchy stress and plastic slip variable per slip system. The simulation also outputs the per grain mean value of these fields. All the results are naturally aligned with the 3D microstructure and imported into the data set through Pymicro. Furthermore, automated meshing functions linking Pymicro's interface with a multi-phase image mesher software developed at Centre des Matériaux [99] were used to mesh both EBSD and DCT reconstructed microstructure. Although these meshes were not used for the present simulation, they are stored within the dataset so that other researchers can access and use them for further analysis.

4.5. Results

Fig. 2.d illustrate the good agreement between simulated and data from the in-situ tensile test, showing that the selected crystal plasticity model and parameters are sound. It should be noted that it is possible to reproduce a single macroscopic curve with different sets of parameters of the crystal plasticity model. Besides, an accurate macroscopic behavior does not guarantee that microscopic plasticity will be accurately captured. Hence, the focus is put hereafter on a detailed comparison at the grain scale between experimental and simulated data within the common region between EBSD and FFT simulation (black frame in Fig. 2.a and b.ii), for the final load step at 1.35% plastic strain. Note that the dataset comprehensively includes records of all experimental and simulation steps for reference.

4.5.1. Slip activity at surface

Out of the 195 segmented grains from the EBSD data at 1.35% post mortem plastic strain, 75 grains with visible active slip on the optical micrograph can be counted (each bullet in Fig. 3.a accounting for detected slip). In addition slip transmission between grains with aligned systems seems to take place. Some of the transmission clusters have been highlighted with black lines connecting the grains involved (this will be analyzed more in detail for some grains of interest in section 4.5.3). It immediately appears that the observed plastic slip intensity varies significantly from a grain to another. Indeed, several parameters can influence the ability to see slip bands. First, the slip direction with respect to free surface has an influence in the first order as grains with slip directions parallel to the surface will have almost no dislocations emerging at the surface which will result in low intensity slip bands even for highly active slip systems. In that regard, the crystallographic texture can play a major role and in the present case, this happens for the prismatic slip directions of all grains with c-axis close to the X-axis direction (grains colored in blue shades on the IPF-Z view, which represent 25% of the grains). Second, it is well known that the principal deformation mode in titanium is the first order prismatic slip [108,109], this considerably reduces the number of available slip systems and apparent slip activity.

This effect is illustrated in section 4.5.3. In addition pure metals are less prone to plastic localization compared to alloys with small shearable precipitates in the bulk of the grains [110,111]. The plastic activity tends to be more homogeneous within the grains where the slip activity is distributed between many different parallel slip planes which lowers in turn the intensity of individual slip bands. A solution to the slip band visibility could be the adoption of high-resolution digital image correlation (HR-DIC) that are able to detect slip bands that form in-plane displacement jumps with a magnitude as low as 10 to 20 nm [112–114]. The observation of surface slip bands also showed that cross-slip appears to be very limited in our case. One explanation is that loading along the rolling direction is the least favorable direction for the apparition of secondary accommodation modes. Under these conditions [115] reported that primary prismatic slip can accommodate on its own most of the deformation without assistance of other mechanisms, mainly by pile-up of dislocations at grain boundaries. This appears to be the case for our experiment suggesting that the contribution of cross-slip can be ignored for the present study.

Some standard features of EBSD commercial and non-commercial solutions have been implemented to centralize data processing and adapt it to the multimodal data structure. Through these capabilities, a multilayered information can be displayed on a single slice of interest of the microstructure. Illustratively, Fig. 3.b.i depicts an EBSD map of the specimen face color-coded with IPF-Z representation, overlaid with prismatic plane traces arbitrarily defined according to Table 3. For practical

Table 3
Identification and color coding of prismatic slip systems.

System ID	Prismatic system	Color
1	$(\bar{1}010)[\bar{1}2\bar{1}0]$	blue
2	$(\bar{1}100)[\bar{1}\bar{1}20]$	yellow
3	$(01\bar{1}0)[2\bar{1}\bar{1}0]$	red

reasons the IPF map obtained from OIM was used. The line thickness directly corresponds to the Schmid factor, visually conveying the probability of slip activation (with thicker lines indicating higher likelihood). The FFT simulation provides slip activity prediction fields, and for ease of comparison with experimental and Schmid factor data, the average activity per grain for each prismatic system was calculated. These values were then correlated with the thickness of the corresponding plane traces (Fig. 3.c). Both maps were generated independently with the same tools in the data platform.

Experimental slip bands and the slip predicted both by the Schmid theory and the FFT show a perfect agreement. Green and cyan grains present the highest slip activity at the surface, while blue grains exhibit comparably limited activity. Note that for each grain, not only the direction of the highest slip activity predicted by the simulation corresponds to the observed slip bands, but the IDs of the systems also match. This can only be achieved if the orientation of the grains for the two modalities are written in the same reference frame and in the fundamental zone. In the present situation all the data was written in the DCT reference frame (X_D, Y_D, Z_D). In general, the slip systems of a given family are physically equivalent but the ID may not correspond as different modalities usually do not share a unique convention to chose the orientation. Pymicro allows to work around this without effort by writing all the orientations in the same reference frame (the DCT in our case) and accounting for the lattice symmetry.

Overall this validates qualitatively the finite strain crystal plasticity model used for this study regarding prediction of the slip activity. Although this was expected as the model relies on the resolved shear stress to activate plasticity, this first step is important to ensure the orientation data has been correctly handled from experimental measurements to the simulation setup. On the other hand the simulation expects the activation of other prismatic systems, more or less intense depending on grains, while no double-slip or cross slip is visible experimentally.

4.5.2. Orientation data

One other metric of interest is the study of the orientation fields. Under crystal finite strain formalism and within the small strain framework, the lattice rotation field gives an estimate of the local dislocation density with the relation:

$$\underset{\sim}{\boldsymbol{\alpha}} \approx -curl(\underset{\sim}{\boldsymbol{R}}^{eT}) \tag{1}$$

here, $\underset{\sim}{\boldsymbol{\alpha}}$ is the dislocation density tensor first introduced by Nye in the scope of small perturbations [116], and $\underset{\sim}{\boldsymbol{R}}^{e}$ is the elastic lattice rotation tensor. Kröner established the link between the Nye tensor and the elastic distortions in the scope of finite strain based on the Lee-Kröner decomposition [117]. Applying the polar decomposition to the elastic deformation gradient in the context of small perturbations leads to Eq. (1). Notice that more recently a modernized treatment has been proposed by Cermelli and Gurtin [118].

The grain reference orientation deviation (GrOD) can also be used to study orientation gradients within grains. It is computed as the misorientation angle of a given pixel/voxel and the mean orientation of the corresponding grain (see appendix A for details on the mean orientation calculation). It is well adapted to moderately deformed microstructures and is used in the following to compare measured and simulated orientations gradients. Other metrics can also be used such as the kernel average misorientation distribution (KAM) or the geometrically necessary dislocations density (ρ_{GND}) as proposed in [119,120]. The GrOD field was computed with Pymicro for both the EBSD and the FFT simulated data (maps respectively displayed in Fig. 4.a.i and Fig. 4.b.i), and were stored into the dataset.

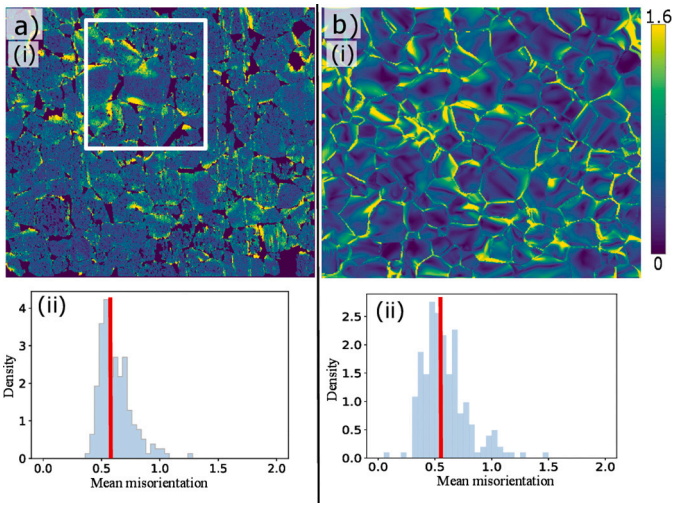

Fig. 4. Intragranular performance assessment of the FFT simulation with respect to the EBSD data. The GrOD data computed with Pymicro is compared to the EBSD measurements at final load. The FFT calculation are performed on 3D aggregates using the DCT reconstructed volume but only surface voxels are depicted. a) EBSD data: (i) Field computed after the OIM segmentation process described in section 4.1, (ii) corresponding histogram of the distribution of average misorientations of each grain over the complete section, b) Simulated data: Field (i) and histogram (ii) obtained from the orientations computed by the simulation for the grains in the EBSD plane. As a reminder, the white frame on a.(i) corresponds to the region of interest (*ROI* that is studied later in section 4.5.3).

Misorientations fields, as a relative metric of orientations are highly sensitive to the diffraction quality as observed for the EBSD data. Especially, the parasitic speckle aforementioned in section 4.1, can artificially increase the local disorientation. To mitigate this issue, the EBSD segmentation was restricted to exclude these area which allows to obtain a consistent GrOD field, at the cost of a sparser field.

Intragranular comparison between the EBSD measured GrOD fields and the FFT predictions at the final load step shows a general agreement with the same order of magnitude in terms of absolute values. On the other hand, while the simulation shows clearly higher activity at the grain boundaries, in line with the crystal plasticity theory which predicts higher dislocation density in these regions, the experimental field suffers from the limited surface quality which hinders clear contrast on most of the map. At the intergranular scale, the histograms of the distribution of average misorientations of each grain over the complete 2D section have a similar shape (see Fig. 4.a.ii and Fig. 4.b.ii). One can notice that effect of the local angular uncertainties from the EBSD disappear when averaging the contributions.

4.5.3. Focus on a region of interest

Experimental analysis: The mechanical analysis is completed by studying the *ROI* region around the grain denoted *5* highlighted in Fig. 2.a. This region appears interesting for several reasons. First, grain 5 and its neighbors display a visible slip activity on the optical micrograph (see Fig. 5.a). Note that the low visibility of the slip traces on the optical micrograph in grains 4, 5 and 6 can be attributed to the respective grain orientations which are such that the direction of the active slip system is almost parallel to the free surface. One can better visualize this configuration on Fig. 6 where the grain is displayed in 3D with its slip systems visible by transparency. Second, the slip traces indicates that some slip transmission may have occurred despite quite different orientation gradients observed at the respective grain boundaries. Finally grain *5* shows

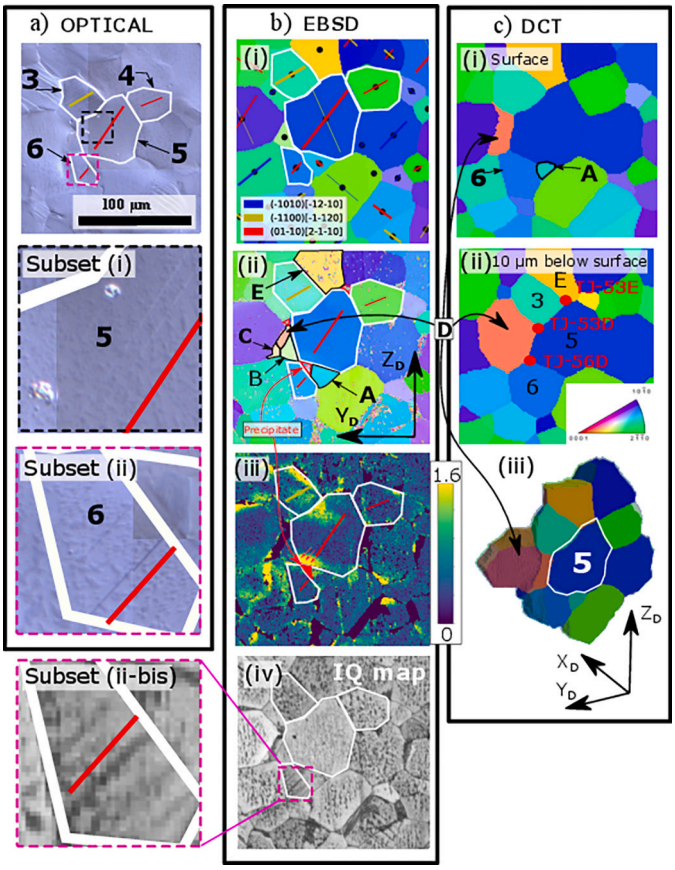

Fig. 5. Experimental multimodal results on the region of interest noted *ROI*: a) Optical data: The subsets (i) and (ii) allow to better visualize the slip bands, b) EBSD data: (i) IPF-Z segmented map overlaid with traces of prismatic slip systems with thickness proportional to their respective Schmid factors - extracted from Fig. 3.b, (ii) Default OIM map, (iii) GrOD field (in degrees) - extracted from Fig. 4.a, (iv) OIM IQ map. The subset (ii-bis) allows to better see the contrasts in the grain *6*, where low IQ bands are aligned with the slip bands. On the views (ii) and (iii) the traces of the active slip systems observed experimentally for the grains of interest *3*, *4*, *5* and *6* are overlaid, c) Digital twin from the DCT reconstruction: (i) View corresponding to the EBSD data, (ii) View 10 µm below the surface. On this view, three triple joints of interest are highlighted (denoted *TJ*), (iii) 3D view of the grain *5* and its immediate neighbors with there morphology and IPF orientations - extracted from Fig. 2.a. Whenever deemed necessary the ids of the grains already identified in Fig. 3.a are recalled. Additional useful grains are also marked for the study, denoted with letters from *A* to *E*.

a high IQ index (see Fig. 5.b.iv) and displays a reliable GrOD field over its entire free surface.

Fig. 5 shows that the slip activity in grain *5* and its neighbors are correctly predicted by the Schmid factor. On the other hand, the grain *5* shows an intense GrOD activity at the boundary with neighbors *3* and *6*, to the contrary of grain *4* (see Fig. 5.b.iii). These boundaries are noted *GB5-3*, *GB5-6* and *GB5-4* in the following. To explain this behavior, a detail examination of the orientations, grain shapes and subsurface microstructure is needed.

By relying on a 2D view only, grain *6* does not seem to be a direct neighbor of grain *5* as a grain labeled *A* appears in between (see EBSD map in Fig. 5.b.i and DCT surface slice in Fig. 5.b.ii). Moreover, the EBSD map reveals the presence of an additional precipitate which steps in at the boundary while the DCT reconstruction ignores this phase (it was instead attributed to grain *6* during the numerical dilation process). But when probing the grains morphology 10 µm below the surface thanks to the digital twin, the grain *A* disappears. This demonstrate that it is actually a very shallow grain (see Fig. 5.c.ii). One can notice that this also holds true for the small surface grains labeled *B* and *C*. A contrario,

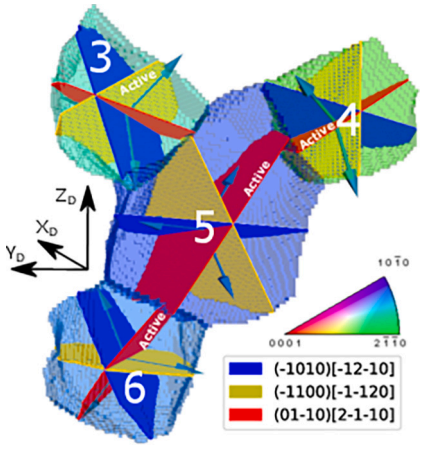

Fig. 6. 3D view of grains *3*, *4*, *5* and *6*, generated with Pymicro. The grains are color coded with the IPF-Z convention in the DCT reference frame. Transparency is set to reveal the prismatic slip systems in the bulk of each grain. The slip planes are colorized according to the convention defined in Table 3. The slip directions are represented with light blue arrows. Active systems observed at the surface are identified with the note *Active*.

the section of grain *6* increases and the common boundary with the grain *5* clearly appears. Idem, the grain noted *D* seems small at the surface whereas it is actually a massive grain underneath. Thereby, the three dimensional analysis of the microstructure prevents interpretation bias contrary to limited information at the surface which can mislead the mechanical analysis.

The inset on the optical micrograph in Fig. 5.a.ii allows to better observe the slip activity of the grain *6*. Notice that for this grain, the slip also leads to strong contrast on the IQ map as shown in the subset Fig. 5.a.ii-bis, which allows to better highlight the ongoing slip activity. The active slip systems *Prism3* (in red) of grains *4*, *5* and *6* are aligned as clearly shown in Fig. 6 and by the m' factors which are respectively 0.73 and 0.70 for *GB5-4* and *GB5-6*, showing that slip transmission is expected (m' close to unity). This seems indeed to take place through *GB5-4* where the plasticity occurs without a significant increase of the GrOD intensity.

The situation is different at the *GB5-6* interface on the side of grain *5* where the GrOD field is intense (see Fig. 5.b.iii). As said, the alignment of prismatic slip systems between the two grains should promote an easy transmission of dislocations and as a result, no significant orientation gradient. By relying only on the EBSD data, the precipitate visible in the surface EBSD seems to preclude the dislocations mobility through the boundary. A first possible interpretation is that dislocations are thus forced to pile-up on the grain boundary and amplify locally the GrOD disorientations field. Moreover, the presence of the massive and disoriented grain *D* leads to a triple joint, noted *TJ-56D*, close to the intense GrOD region. It is likely that this grain contributes to the formation of incompatible strain fields which could disturb the dislocations motion, and even be the cause of stress concentrations which could lead to active dislocation sources in the neighboring grain. Ultimately, it may contribute to the intense GrOD activity observed. As such, slip transmission is not a trivial mechanism. In the present case, it seems more likely to take place beneath the surface when moving away from the precipitate.

Eventually a third configuration can be looked at with the *GB5-3* interface. Once again, the strong GrOD activity measured is mainly concentrated on the grain *5* side. This time the active systems at surface are not aligned while no precipitate appears in the observed section. In this case, the accumulation of dislocations by slip can be explained partly by the activation of the *Prism2* system (with a Schmid factor of 0.36, depicted in yellow on Fig. 5.b.i and Fig. 6) which can be blocked at the *GB5-3* boundary (m' factor below 0.21). One can else notice that grain *D* is also present at the triple joint *TJ-53D* and the grain *E* defines an ad-

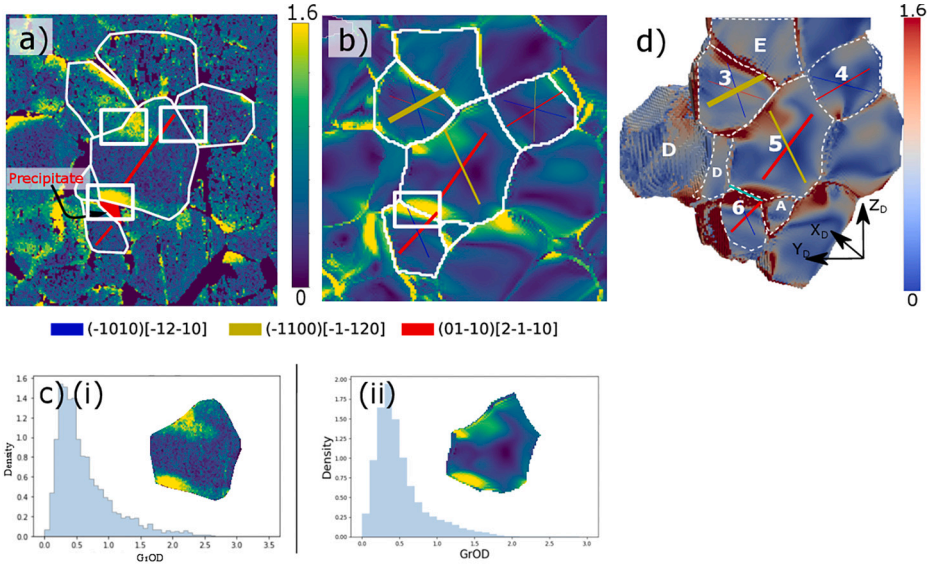

Fig. 7. Performance assessment of the FFT simulation (b and c) with respect to the EBSD experimental data (a). Here the GrOD field (in degrees) is compared in the region of interest *ROI* at the final load state: a) EBSD field, b) Slice of the FFT field, c) Statistical mosaicity comparison between EBSD (i) and FFT data (ii) for the grain *5*, d) FFT field in 3D for the grain *5* and its immediate neighbors (with a default Paraview scalebar). On each modality, the corresponding slip activity observed on the grains of interest *3*, *4*, *5* and *6* is once again overlaid. The absence of precipitates in the digital twin leads to a wrong prediction of the simulation (dotted red frame). Elsewhere a the interfaces of grain *5*, the numerical prediction performs well (full line white frames).

ditional triple junction *JT-53E*. Grain *3* is therefore surrounded by two strongly disoriented grains. The identified triple junctions are precisely located on both sides of the intense GrOD domain and may activate dislocations sources contributing to increase locally the GrOD field.

Simulation results: The simulation is now compared to the experimental analysis in the *ROI* of the EBSD face. Fig. 7 shows, side by side, the experimental and simulated GrOD fields in (a) and (b). In addition, the 3D simulated GrOD field of grain *5* and its immediate neighbors is shown in (d). Once again, in each view, the traces of active prismatic slip systems are superimposed for grains *3* to *6*.

First, in line with the observations in the full map, the systems with the highest activity in the simulation match perfectly with those actually observed. The simulation also reveals a competition between the active slip systems. For instance, intense double slip between *Prism3* (in red) and *Prism2* (in yellow) is predicted in the grain *5* (respectively 0.017 and 0.012 cumulated slip). This mechanism, which can be explained by the favorable orientation of both systems with respect to the load (respective Schmid factors are 0.47 and 0.38), is not directly accessible with the experimental data at hands, as the *Prism2* slip direction is parallel to the surface and thus not visible from the slip traces.

Looking at the intragranular scale, the simulation also reproduces correctly the GrOD field observed experimentally, especially at the boundaries of interest. First, turning our attention to *GB5-6*, the intense GrOD activity on the side of the grain *5* is very well reproduced by the simulation. A strong activity also clearly appears on the side of the grain *6*, which is also seen in the EBSD data, although with a lower intensity. As the simulation does not include the precipitates, this result does not support a strong influence of the precipitates but rather a predominant role of the local arrangements of the grains. A closer look at the individual prismatic slip fields provided by the simulation (not displayed here) gives even more insight. As said previously, *Prism3* and *Prism2* compete at a similar magnitude globally in grain *5*, but locally, close to *GB5-6*, *Prism2* largely dominates over *Prism3*. This demonstrates a strong local deviation from the Schmid factor prediction as the complex 3D arrangement leads to a local mechanical equilibrium more favorable to *Prism2*. The presence of the grain *D* in the immediate neighborhood might influence this configuration. As a result, the mechanical states impedes the slip transmission between grains *5* and *6*, leading to strong local misorientations. In future experiments, high resolution DIC surface measurements could be used to cross-validate the multiple slip predicted by the simulation such, as reported in [121].

Similar distribution of slip is observed at *GB5-4*. The *Prism3* activity in the grain *5* also vanishes close to the boundary, substituted by *Prism2*. But as the grain *4* has a much less favorable orientation with respect to the load, the overall slip activity in the region is limited which, in turn, leads to limited GrOD activity. Once again, the apparent slip transmission identified from the experimental data is challenged by the simulation.

4.5.4. Discussion and prospects

Overall, the simulation demonstrates a satisfying performance at the intergranular an intragranular scales, the slip system activity and GrOD fields are well predicted using the experimental 3D microstructure as input. The detailed analysis of grain 5 and its neighborhood showed that precipitates seem to have a non negligible influence on the local prediction of the plasticity behavior of the simulation. Similar conclusions can be drawn in other location, although some difficulty in the EBSD preparation had made the analysis more complex. Based on the simulation results, the data can be further processed for instance by computing the geometrically necessary dislocations density ρ_{GND} from the lattice rotation field. This can then be used to supplement the experimental data in the analysis of the plasticity mechanisms.

The data set can be further completed by additional modalities. Performing a series of post deformation DCT scans (although this would be limited to low level of deformation, typically below 2% strain) on the same volume would allow to reconstruct the lattice rotation field in the bulk and study the accumulation of GNDs. Presently, this information can only be accessed via the simulation results. If planned in advanced, one could consider to perform non destructive measurements such as HR-DIC [114] to get access to the intragranular elastic strain field and individual slip system activation at the surface [121], or in the bulk with digital volume correlation (DVC - not applicable to the present material). Higher resolution non destructive methods can also be leveraged such as Dark Field X-ray Microscopy (DFXM) [122] or scanning-3DXRD [44].

5. Summary

Data management will play a central role in the development and diffusion of high-throughput multimodal methodologies for material science. To support their development, the associated management tools must meet specific requirements: implement versatile data formats and standards shared by the scientific community, ensure scalable, hierarchical and self-documented data storage, and promote automated integration with modeling and experiments numerical tools. The data platform presented in this work has been implemented in accordance with these guidelines within the Pymicro package. It enables to merge together microstructural, micromechanical and statistical data attached to the same material sample, coming from 2D and 3D characterization techniques, as well as numerical simulation tools, geometrically supported by images or meshes. The platform has been integrated with electron microscopy and X-ray tomography standard formats, with an FFT-based and a finite element mechanical solvers, and an automated meshing tool. It furthermore provides an efficient, unified and user-friendly tool for building, browsing and visualizing large-scale datasets that bring together this rich diversity of data.

The Pymicro data platform has been used to process and build a dataset associated to a grade 2 titanium tensile specimen. This highly multimodal dataset gathers data from three different imaging modalities: DCT, EBSD and optical microscopy, from a numerical simulation, and the tensile test stress-strain measurement. A large variety of information is included in the dataset, such as grains orientation maps, grains orientation deviation fields, simulated stress, lattice rotation and plasticity fields. The platform also enabled registration of 2D and 3D data maps (see [105] for instance), and automated generation of simulation input data for the FFT-based solver AMITEX_FFTP. The convergence of all data items allows to produce a wide variety of visualizations and comparisons of statistical and grain-to-grain data, from simulations and experiments, while interacting solely with the data platform.

Overall, this work is a contribution towards the facilitation, automation and acceleration of cross-analysis operations involving massive and diversified data for the mechanics of polycrystalline materials. In comparison with multimodal datasets published in the literature, its originality lies in the convergence of measured and simulated data format, which enables easy and robust cross-comparisons of models with experiments. It paves the way for application to sophisticated tasks such as the identification of micromechanical models through comparison of micron-scale mechanical heterogeneities, or the training of machine learning models relying on measured and simulated microstructural and mechanical datasets, to predict the evolution of damage at the micron scale in polycrystals. Finally, in line with other contributions [46,74], this work also aims to advocate for the establishment of standards for microstructural data management within the mechanics of materials community.

CRediT authorship contribution statement

Aldo Marano: Writing – original draft, Software, Methodology, Conceptualization. **Clément Ribart:** Writing – original draft, Investigation, Data curation. **Henry Proudhon:** Writing – review & editing, Software, Project administration, Funding acquisition, Data curation, Conceptualization.

Declaration of competing interest

The authors declare that they have no known competing financial interests or personal relationships that could have appeared to influence the work reported in this paper.

Data availability

The consolidated data set constructed using Pymicro and the different modalities, including the FFT simulation fields, is available from Zenodo [123]. The methods used to process the different modalities presented in section 4 are available from computational notebooks to reproduce the results obtained via EBSD [93], DCT characterization [94] and CP-FFT analysis [95].

Acknowledgements

HP would like to acknowledge funding through the BIGMECA chair of Fondation MINES Paris under the patronage of Safran. The authors are grateful to ESRF for providing beam time through long term proposal MA-4925 and to Wolfgang Ludwig for his help with the DCT acquisition. HP and CR would also like to thank the workshop and the micromax support team at Centre des Matériaux for help with the EBSD in situ tensile test. This project was provided with computing HPC and storage resources by GENCI at IDRIS within allocation A9-A0090911901 on the supercomputer Jean Zay's V100 partition.

Appendix A. Computing mean grain orientations

The grain orientations are defined as passive rotations that bring the chosen reference frame (here the sample reference frame XYZ) in coincidence with the reference frame attached to the crystal lattice. Several descriptors can be used to define mathematically rotations such as Euler angles, Rodrigues vectors, axis/angle representations or quaternions, as nicely summarized in [124].

Averaging orientation can conveniently be achieved by averaging quaternions provided one takes care of material symmetries. Indeed, depending on the lattice symmetry, several orientations are physically equivalent ($n_{sym} = 12$ for the present hexagonal case, 24 for the cubic case). This is usually handled by moving orientations to the fundamental zone but problem may arise when the mean orientation is close to the border of the fundamental zone and if the orientation data representing the orientation spread crosses the boundary. To work around this issue, several strategies can be used, one can chose one of the orientation point as a reference as proposed in [125]. In Pymicro the strategy is slightly different. It consists in computing all equivalent rotations for all data points in quaternion space which results in n_{sym} clusters that are automatically labeled by k-means clustering. The average orientation is then computed for each cluster and the mean orientation that lies in the fundamental zone is retained. Note that this should not be done in Rodrigues space using an euclidean distance metric since the non linearity with the rotation angle may break the clustering step.

References

[1] Yang Chen, Lionel Gélébart, Camille Chateau, Michel Bornert, Cédric Sauder, Andrew King, Analysis of the damage initiation in a sic/sic composite tube from a direct comparison between large-scale numerical simulation and synchrotron x-ray micro-computed tomography, Int. J. Solids Struct. (ISSN 0020-7683) 161 (4) (2019), https://doi.org/10.1016/j.ijsolstr.2018.11.009.

[2] F. Di Gioacchino, J. Quinta Da Fonseca, Plastic strain mapping with sub-micron resolution using digital image correlation, Exp. Mech. 53 (5) (2013) 743–754.

[3] C.B. Montgomery, B. Koohbor, N.R. Sottos, A robust patterning technique for electron microscopy-based digital image correlation at sub-micron resolutions, Exp. Mech. 59 (7) (2019) 1063–1073.

[4] Angus J. Wilkinson, Graham Meaden, David J. Dingley, High-resolution elastic strain measurement from electron backscatter diffraction patterns: new levels of sensitivity, Ultramicroscopy 106 (4–5) (2006) 307–313.

[5] A.J. Wilkinson, E.E. Clarke, T.B. Britton, P. Littlewood, P.S. Karamched, High-resolution electron backscatter diffraction: an emerging tool for studying local deformation, J. Strain Anal. Eng. Des. 45 (5) (2010) 365–376.

[6] M. Pitaval, P. Morin, J. Baudry, E. Vicario, G. Fontaine, Advances in crystalline contrast from defects, in: Scanning Electron Microscopy/1977/I, IIT Research Institute, Chicago, Ill, 1977, pp. 439–444.

[7] Stefan Zaefferer, Nahid-Nora Elhami, Theory and application of electron channelling contrast imaging under controlled diffraction conditions, Acta Mater. 75 (2014) 20–50.

[8] J.M. Teixeira Pinto, F. Touchard, S. Castagnet, C. Nadot-Martin, D. Mellier, Dic strain measurements at the micro-scale in a semi-crystalline polymer, Exp. Mech. (ISSN 0014-4851) 53 (2013) 10, https://doi.org/10.1007/s11340-013-9753-2.

[9] B. Wisner, A. Kontsos, In situ monitoring of particle fracture in aluminium alloys, Fatigue Fract. Eng. Mater. Struct. 41 (3) (2018) 581–596.
[10] Muhamad Fatikul Arif, Fodil Meraghni, Yves Chemisky, Nicolas Despringre, Gilles Robert, In situ damage mechanisms investigation of pa66/gf30 composite: effect of relative humidity, Composites, Part B, Eng. 58 (2014) 487–495.
[11] D.J. Mortell, D.A. Tanner, C.T. McCarthy, In-situ sem study of transverse cracking and delamination in laminated composite materials, Compos. Sci. Technol. 105 (2014) 118–126.
[12] Yuhei Ogawa, Domas Birenis, Hisao Matsunaga, Annett Thøgersen, Øystein Prytz, Osamu Takakuwa, Junichiro Yamabe, Multi-scale observation of hydrogen-induced, localized plastic deformation in fatigue-crack propagation in a pure iron, Scr. Mater. (ISSN 1359-6462) 140 (2017) 11, https://doi.org/10.1016/j.scriptamat.2017.06.037.
[13] P.F. Gao, Z.N. Lei, X.X. Wang, M. Zhan, Deformation in fatigue crack tip plastic zone and its role in crack propagation of titanium alloy with tri-modal microstructure, Mater. Sci. Eng. A (ISSN 0921-5093) 739 (2019) 1, https://doi.org/10.1016/j.msea.2018.10.049.
[14] Xiangnan Pan, Hang Su, Chengqi Sun, Youshi Hong, The behavior of crack initiation and early growth in high-cycle and very-high-cycle fatigue regimes for a titanium alloy, Int. J. Fatigue (ISSN 0142-1123) 115 (2018) 10, https://doi.org/10.1016/j.ijfatigue.2018.03.021.
[15] Changsheng Tan, Qiaoyan Sun, Lin Xiao, Yongqing Zhao, Jun Sun, Characterization of deformation in primary alpha phase and crack initiation and propagation of tc21 alloy using in-situ sem experiments, Mater. Sci. Eng. A (ISSN 0921-5093) 725 (2018) 5, https://doi.org/10.1016/j.msea.2018.03.123.
[16] Di Wan, Yun Deng, Jan Inge Hammer Meling, Antonio Alvaro, Afrooz Barnoush, Hydrogen-enhanced fatigue crack growth in a single-edge notched tensile specimen under in-situ hydrogen charging inside an environmental scanning electron microscope, Acta Mater. (ISSN 1359-6454) 170 (2019) 5, https://doi.org/10.1016/j.actamat.2019.03.032.
[17] Fabio Di Gioacchino, João Quinta da Fonseca, An experimental study of the polycrystalline plasticity of austenitic stainless steel, Int. J. Plast. 74 (2015) 92–109.
[18] S. Hémery, P. Nizou, P. Villechaise, In situ sem investigation of slip transfer in ti-6al-4v: effect of applied stress, Mater. Sci. Eng. A (ISSN 0921-5093) 709 (2018) 277, https://doi.org/10.1016/j.msea.2017.10.058.
[19] Z. Chen, S.H. Daly, Active slip system identification in polycrystalline metals by digital image correlation (dic), Exp. Mech. 57 (1) (2017) 115–127.
[20] Thomas Edward James Edwards, Fabio Di Gioacchino, Amy Jane Goodfellow, William John Clegg, Slip bands in lamellar tial during high cycle fatigue microcompression by correlative total strain mapping, diffraction orientation mapping and transmission electron imaging, Int. J. Fatigue (ISSN 0142-1123) 124 (2019) 7, https://doi.org/10.1016/j.ijfatigue.2019.03.016.
[21] Ryan Sperry, Songyang Han, Zhe Chen, Samantha H. Daly, Martin A. Crimp, David T. Fullwood, Comparison of ebsd, dic, afm, and ecci for active slip system identification in deformed ti-7al, Mater. Charact. 173 (2021) 110941.
[22] F. Bourdin, J.C. Stinville, M.P. Echlin, P.G. Callahan, W.C. Lenthe, C.J. Torbet, D. Texier, F. Bridier, J. Cormier, P. Villechaise, T.M. Pollock, V. Valle, Measurements of plastic localization by heaviside-digital image correlation, Acta Mater. (ISSN 1359-6454) 157 (2018) 307–325, https://doi.org/10.1016/j.actamat.2018.07.013.
[23] X. Xu, D. Lunt, R. Thomas, R. Prasath Babu, A. Harte, M. Atkinson, J.Q. Da Fonseca, M. Preuss, Identification of active slip mode in a hexagonal material by correlative scanning electron microscopy, Acta Mater. (ISSN 1359-6454) 175 (2019) 376–393, https://doi.org/10.1016/j.actamat.2019.06.024.
[24] Xiaojiao You, Jian Yang, Chengyi Dan, Qiwei Shi, Shengyi Zhong, Haowei Wang, Zhe Chen, Statistical analysis of slip transfer in al alloy based on in-situ tensile test and high-throughput computing method, Int. J. Plast. 166 (2023) 103649.
[25] Haoyu Hu, Fabien Briffod, Takayuki Shiraiwa, Manabu Enoki, Automated slip system identification and strain analysis framework using high-resolution digital image correlation data: application to a bimodal ti-6al-4v alloy, Int. J. Plast. 166 (2023) 103618.
[26] M.A. Charpagne, J.C. Stinville, P.G. Callahan, Damien Texier, Z. Chen, P. Villechaise, Valery Valle, T.M. Pollock, Automated and quantitative analysis of plastic strain localization via multi-modal data recombination, Mater. Charact. 163 (2020) 110245.
[27] R.L. Black, T. Garbowski, C. Bean, A.L. Eberle, S. Nickell, Damien Texier, V. Valle, J.C. Stinville, High-throughput high-resolution digital image correlation measurements by multi-beam sem imaging, Exp. Mech. (2023) 1–15.
[28] J.H. Liu, N. Vanderesse, J-C. Stinville, T.M. Pollock, P. Bocher, Damien Texier, In-plane and out-of-plane deformation at the sub-grain scale in polycrystalline materials assessed by confocal microscopy, Acta Mater. 169 (2019) 260–274.
[29] Wujun Yin, Fabien Briffod, Haoyu Hu, Takayuki Shiraiwa, Manabu Enoki, Three-dimensional configuration of crystal plasticity in stainless steel assessed by high resolution digital image correlation and confocal microscopy, Int. J. Plast. 170 (2023) 103762.
[30] Michael A. Groeber, B.K. Haley, Michael D. Uchic, Dennis M. Dimiduk, Somnath Ghosh, 3d reconstruction and characterization of polycrystalline microstructures using a fib–sem system, Mater. Charact. 57 (4–5) (2006) 259–273.
[31] Michael Groeber, Somnath Ghosh, Michael D. Uchic, Dennis M. Dimiduk, A framework for automated analysis and simulation of 3d polycrystalline microstructures.: Part 1: statistical characterization, Acta Mater. 56 (6) (2008) 1257–1273.
[32] Joshua A. Taillon, Christopher Pellegrinelli, Yi-Lin Huang, Eric D. Wachsman, Lourdes G. Salamanca-Riba, Improving microstructural quantification in fib/sem nanotomography, Ultramicroscopy 184 (2018) 24–38.
[33] José David Arregui-Mena, Philip D. Edmondson, Anne A. Campbell, Yutai Katoh, Site specific, high-resolution characterisation of porosity in graphite using fib-sem tomography, J. Nucl. Mater. 511 (2018) 164–173.
[34] Philip J. Withers, Michael Preuss, Fatigue and damage in structural materials studied by x-ray tomography, Annu. Rev. Mater. Res. 42 (2012) 81–103.
[35] Thilo F. Morgeneyer, Thibault Taillandier-Thomas, Lukas Helfen, Tilo Baumbach, Ian Sinclair, Stéphane Roux, François Hild, In situ 3-d observation of early strain localization during failure of thin al alloy (2198) sheet, Acta Mater. 69 (2014) 78–91.
[36] Eric Maire, Thilo Morgeneyer, Caroline Landron, Jerome Adrien, Lukas Helfen, Bulk evaluation of ductile damage development using high resolution tomography and laminography, C. R. Phys. 13 (3) (2012) 328–336.
[37] Eric Maire, Christophe Le Bourlot, Jérôme Adrien, Andreas Mortensen, Rajmund Mokso, 20 hz x-ray tomography during an in situ tensile test, Int. J. Fract. 200 (1) (2016) 3–12.
[38] Maxime Pelerin, Andrew King, Lucien Laiarinandrasana, Henry Proudhon, Development of a versatile mechanical testing device for in situ synchrotron tomography and diffraction experiments, Integr. Mater. Manuf. Innov. 8 (3) (2019) 378–387.
[39] Péter Reischig, Andrew King, Laura Nervo, Nicola Viganó, Yoann Guilhem, Willem Jan Palenstijn, KJoost Batenburg, Michael Preuss, Wolfgang Ludwig, Advances in x-ray diffraction contrast tomography: flexibility in the setup geometry and application to multiphase materials, J. Appl. Crystallogr. 46 (2) (2013) 297–311.
[40] Florian Bachmann, Hrishikesh Bale, Nicolas Gueninchault, Christian Holzner, Erik Mejdal Lauridsen, 3d grain reconstruction from laboratory diffraction contrast tomography, J. Appl. Crystallogr. 52 (3) (2019) 643–651.
[41] Yujiro Hayashi, Yoshiharu Hirose, Yoshiki Seno, Polycrystal orientation mapping using scanning three-dimensional x-ray diffraction microscopy, J. Appl. Crystallogr. 48 (4) (2015) 1094–1101.
[42] K. Chatterjee, A. Venkataraman, T. Garbaciak, J. Rotella, M.D. Sangid, A.J. Beaudoin, P. Kenesei, J.S. Park, A.L. Pilchak, Study of grain-level deformation and residual stresses in ti-7al under combined bending and tension using high energy diffraction microscopy (hedm), Int. J. Solids Struct. 94 (2016) 35–49.
[43] Jay C. Schuren, Paul A. Shade, Joel V. Bernier, Shiu Fai Li, Basil Blank, Jonathan Lind, Peter Kenesei, Ulrich Lienert, Robert M. Suter, Todd J. Turner, et al., New opportunities for quantitative tracking of polycrystal responses in three dimensions, Curr. Opin. Solid State Mater. Sci. 19 (4) (2015) 235–244.
[44] N. Axel Henningsson, Stephen A. Hall, Jonathan P. Wright, Johan Hektor, Reconstructing intragranular strain fields in polycrystalline materials from scanning 3dxrd data, J. Appl. Crystallogr. 53 (2) (2020) 314–325.
[45] Henry Proudhon, Nicolas Guéninchault, Samuel Forest, Wolfgang Ludwig, Incipient bulk polycrystal plasticity observed by synchrotron in-situ topotomography, Materials 11 (10) (2018).
[46] Henry Proudhon, Maxime Pelerin, Andrew King, Wolfgang Ludwig, In situ 4d mechanical testing of structural materials: the data challenge, Curr. Opin. Solid State Mater. Sci. (ISSN 1359-0286) 24 (2020), https://doi.org/10.1016/j.cossms.2020.100834.
[47] Minh Tien Tran, Xuan Minh Nguyen, Hyunki Kim, Hobyung Chae, Wanchuck Woo, Ho Won Lee, Dong-Kyu Kim, Micromechanical properties and deformation behavior of the constituent phases in 3rd generation complex phase ahss: in-situ neutron experiment and crystal plasticity simulation, Int. J. Plast. (2023) 103812.
[48] J.C. Stinville, J.M. Hestroffer, M.A. Charpagne, A.T. Polonsky, M.P. Echlin, C.J. Torbet, V. Valle, K.E. Nygren, M.P. Miller, O. Klaas, et al., Multi-modal dataset of a polycrystalline metallic material: 3d microstructure and deformation fields, Sci. Data 9 (1) (2022) 460.
[49] Sven E. Gustafson, Wolfgang Ludwig, Raquel Rodriguez-Lamas, Can Yildirim, Katherine S. Shanks, Carsten Detlefs, Michael D. Sangid, Revealing 3d intragranular micromechanical fields at triple junctions, Acta Mater. 260 (2023) 119300.
[50] J.C. Stinville, W. Ludwig, P.G. Callahan, M.P. Echlin, V. Valle, T.M. Pollock, H. Proudhon, Observation of bulk plasticity in a polycrystalline titanium alloy by diffraction contrast tomography and topotomography, Mater. Charact. 188 (2022) 111891.
[51] D.J. Shadle, K.E. Nygren, J.C. Stinville, M.A. Charpagne, T.J.H. Long, M.P. Echlin, C.J. Budrow, A.T. Polonsky, T.M. Pollock, I.J. Beyerlein, et al., Integrating in-situ multi-modal characterizations with signatures to investigate localized deformation, Mater. Charact. 205 (2023) 113332.
[52] Romain Quey, P.R. Dawson, Fabrice Barbe, Large-scale 3d random polycrystals for the finite element method: generation, meshing and remeshing, Comput. Methods Appl. Mech. Eng. 200 (17–20) (2011) 1729–1745.
[53] Michael A. Groeber, Michael A. Jackson, Dream. 3d: a digital representation environment for the analysis of microstructure in 3d, Integr. Mater. Manuf. Innov. 3 (1) (2014) 56–72.
[54] Ashley D. Spear, Jacob D. Hochhalter, Albert R. Cerrone, Shiu Fai Li, Jonathan F. Lind, Robert M. Suter, Anthony R. Ingraffea, A method to generate conformal finite-element meshes from 3d measurements of microstructurally small fatigue-crack propagation, Fatigue Fract. Eng. Mater. Struct. 39 (6) (2016) 737–751.
[55] Swantje Bargmann, Benjamin Klusemann, Jürgen Markmann, Jan Eike Schnabel, Konrad Schneider, Celal Soyarslan, Jana Wilmers, Generation of 3d representative

volume elements for heterogeneous materials: a review, Prog. Mater. Sci. 96 (2018) 322–384.
[56] Clémence Petit, Eric Maire, Sylvain Meille, Jérôme Adrien, Two-scale study of the fracture of an aluminum foam by x-ray tomography and finite element modeling, Mater. Des. 120 (2017) 117–127.
[57] Harris Farooq, Georges Cailletaud, Samuel Forest, David Ryckelynck, Crystal plasticity modeling of the cyclic behavior of polycrystalline aggregates under non-symmetric uniaxial loading: global and local analyses, Int. J. Plast. 126 (2020) 102619.
[58] Robert M. Auenhammer, Lars P. Mikkelsen, Leif E. Asp, Brina J. Blinzler, Automated x-ray computer tomography segmentation method for finite element analysis of non-crimp fabric reinforced composites, Compos. Struct. 256 (2021) 113136.
[59] Ricardo A. Lebensohn, Anand K. Kanjarla, Philip Eisenlohr, An elasto-viscoplastic formulation based on fast Fourier transforms for the prediction of micromechanical fields in polycrystalline materials, Int. J. Plast. 32 (2012) 59–69.
[60] Yang Chen, Lionel Gélébart, Camille Chateau, Michel Bornert, Cédric Sauder, Andrew King, Analysis of the damage initiation in a sic/sic composite tube from a direct comparison between large-scale numerical simulation and synchrotron x-ray micro-computed tomography, Int. J. Solids Struct. 161 (2019) 111–126.
[61] Romain Charière, Aldo Marano, Lionel Gélébart, Use of composite voxels in fft based elastic simulations of hollow glass microspheres/polypropylene composites, Int. J. Solids Struct. 182 (2020) 1–14.
[62] Andrea Rovinelli, Henry Proudhon, Ricardo A. Lebensohn, Michael D. Sangid, Assessing the reliability of fast Fourier transform-based crystal plasticity simulations of a polycrystalline material near a crack tip, Int. J. Solids Struct. 184 (2020) 153–166.
[63] Jonathan M. Hestroffer, Jean-Charles Stinville, Marie-Agathe Charpagne, Matthew P. Miller, Tresa M. Pollock, Irene J. Beyerlein, Slip localization behavior at triple junctions in nickel-base superalloys, Acta Mater. 249 (2023) 118801.
[64] Paul A. Shade, William D. Musinski, Mark Obstalecki, Darren C. Pagan, Armand J. Beaudoin, Joel V. Bernier, Todd J. Turner, Exploring new links between crystal plasticity models and high-energy x-ray diffraction microscopy, Curr. Opin. Solid State Mater. Sci. 23 (5) (2019) 100763.
[65] Veerappan Prithivirajan, Priya Ravi, Diwakar Naragani, Michael D. Sangid, Direct comparison of microstructure-sensitive fatigue crack initiation via crystal plasticity simulations and in situ high-energy x-ray experiments, Mater. Des. 197 (2021) 109216.
[66] A.J. Beaudoin, M. Obstalecki, R. Storer, W. Tayon, J. Mach, P. Kenesei, U. Lienert, Validation of a crystal plasticity model using high energy diffraction microscopy, Model. Simul. Mater. Sci. Eng. 20 (2) (2012) 024006.
[67] Adrien Guery, François Hild, Félix Latourte, Stéphane Roux, Identification of crystal plasticity parameters using dic measurements and weighted femu, Mech. Mater. 100 (2016) 55–71.
[68] M.P. Miller, P.R. Dawson, Understanding local deformation in metallic polycrystals using high energy x-rays and finite elements, Curr. Opin. Solid State Mater. Sci. 18 (5) (2014) 286–299.
[69] Su Leen Wong, Mark Obstalecki, Matthew P. Miller, Paul R. Dawson, Stress and deformation heterogeneity in individual grains within polycrystals subjected to fully reversed cyclic loading, J. Mech. Phys. Solids 79 (2015) 157–185.
[70] Henry Proudhon, Jia Li, Peter Reischig, Nicolas Guéninchault, Samuel Forest, Wolfgang Ludwig, Coupling diffraction contrast tomography with the finite element method, Adv. Eng. Mater. 18 (6) (2016) 903–912.
[71] Andrea Rovinelli, Michael D. Sangid, Henry Proudhon, Yoann Guilhem, Ricardo A. Lebensohn, Wolfgang Ludwig, Predicting the 3d fatigue crack growth rate of small cracks using multimodal data via Bayesian networks: in-situ experiments and crystal plasticity simulations, J. Mech. Phys. Solids 115 (2018) 208–229.
[72] David Ryckelynck, Djamel Missoum Benziane, Hyper-reduction framework for model calibration in plasticity-induced fatigue, Adv. Model. Simul. Eng. Sci. 3 (1) (2016) 1–16.
[73] Elena Lopez, David Gonzalez, J.V. Aguado, Emmanuelle Abisset-Chavanne, Elias Cueto, Christophe Binetruy, Francisco Chinesta, A manifold learning approach for integrated computational materials engineering, Arch. Comput. Methods Eng. 25 (1) (2018) 59–68.
[74] Daniel S. Gianola, Nicolò Maria della Ventura, Glenn H. Balbus, Patrick Ziemke, McLean P. Echlin, Matthew R. Begley, Advances and opportunities in high-throughput small-scale mechanical testing, Curr. Opin. Solid State Mater. Sci. 27 (4) (2023) 101090.
[75] N.R. Brodnik, C. Muir, N. Tulshibagwale, J. Rossin, M.P. Echlin, C.M. Hamel, S.L.B. Kramer, T.M. Pollock, J.D. Kiser, C. Smith, et al., Perspective: machine learning in experimental solid mechanics, J. Mech. Phys. Solids 173 (2023) 105231.
[76] Marat I. Latypov, Amil Khan, Christian A. Lang, Kris Kvilekval, Andrew T. Polonsky, McLean P. Echlin, Irene J. Beyerlein, B.S. Manjunath, Tresa M. Pollock, Bisque for 3d materials science in the cloud: microstructure–property linkages, Integr. Mater. Manuf. Innov. 8 (1) (2019) 52–65.
[77] François Bonnarel, Pierre Fernique, Olivier Bienaymé, Daniel Egret, Françoise Genova, Mireille Louys, François Ochsenbein, Marc Wenger, James G. Bartlett, The aladin interactive sky atlas-a reference tool for identification of astronomical sources, Astron. Astrophys. Suppl. Ser. 143 (1) (2000) 33–40.
[78] Marc Wenger, François Ochsenbein, Daniel Egret, Pascal Dubois, François Bonnarel, Suzanne Borde, Françoise Genova, Gérard Jasniewicz, Suzanne Laloë, Soizick Lesteven, et al., The simbad astronomical database-the cds reference database for astronomical objects, Astron. Astrophys. Suppl. Ser. 143 (1) (2000) 9–22.
[79] Kristian Kvilekval, Dmitry Fedorov, Boguslaw Obara, Ambuj Singh, B.S. Manjunath, Bisque: a platform for bioimage analysis and management, Bioinformatics 26 (4) (2010) 544–552.
[80] Committee on Integrated Computational Materials Engineering, Integrated Computational Materials Engineering: a Transformational Discipline for Improved Competitiveness and National Security, National Academies Press, Washington, DC, 2008.
[81] Juan J. de Pablo, Barbara Jones, Cora Lind Kovacs, Vidvuds Ozolins, Arthur P. Ramirez, The materials genome initiative, the interplay of experiment, theory and computation, Curr. Opin. Solid State Mater. Sci. 18 (2) (2014) 99–117.
[82] Stefano Curtarolo, Wahyu Setyawan, Gus L.W. Hart, Michal Jahnatek, Roman V. Chepulskii, Richard H. Taylor, Shidong Wang, Junkai Xue, Kesong Yang, Ohad Levy, et al., Aflow: an automatic framework for high-throughput materials discovery, Comput. Mater. Sci. 58 (2012) 218–226.
[83] Stefano Curtarolo, Wahyu Setyawan, Shidong Wang, Junkai Xue, Kesong Yang, Richard H. Taylor, Lance J. Nelson, Gus L.W. Hart, Stefano Sanvito, Marco Buongiorno-Nardelli, et al., Aflowlib. org: a distributed materials properties repository from high-throughput ab initio calculations, Comput. Mater. Sci. 58 (2012) 227–235.
[84] Richard H. Taylor, Frisco Rose, Cormac Toher, Ohad Levy, Kesong Yang, Marco Buongiorno Nardelli, Stefano Curtarolo, A restful api for exchanging materials data in the aflowlib. org consortium, Comput. Mater. Sci. 93 (2014) 178–192.
[85] Anubhav Jain, Shyue Ping Ong, Geoffroy Hautier, Wei Chen, William Davidson Richards, Stephen Dacek, Shreyas Cholia, Dan Gunter, David Skinner, Gerbrand Ceder, et al., Commentary: the materials project: a materials genome approach to accelerating materials innovation, APL Mater. 1 (1) (2013) 011002.
[86] Casper W. Andersen, Rickard Armiento, Evgeny Blokhin, Gareth J. Conduit, Shyam Dwaraknath, Matthew L. Evans, Ádám Fekete, Abhijith Gopakumar, Saulius Gražulis, Andrius Merkys, et al., Optimade: an api for exchanging materials data, arXiv preprint arXiv:2103.02068, 2021.
[87] Duncan N. Johnstone, H. Ben Martineau, Phillip Crout, Paul A. Midgley, Alexander S. Eggeman, Density-based clustering of crystal (mis)orientations and the *orix* Python library, J. Appl. Crystallogr. 53 (5) (Oct 2020) 1293–1298, https://doi.org/10.1107/S1600576720011103.
[88] Mark Könnecke, Frederick A. Akeroyd, Herbert J. Bernstein, Aaron S. Brewster, Stuart I. Campbell, Björn Clausen, Stephen Cottrell, Jens Uwe Hoffmann, Pete R. Jemian, David Männicke, et al., The nexus data format, J. Appl. Crystallogr. 48 (1) (2015) 301–305.
[89] Andrew T. Polonsky, Christian A. Lang, Kristian G. Kvilekval, Marat I. Latypov, McLean P. Echlin, B.S. Manjunath, Tresa M. Pollock, Three-dimensional analysis and reconstruction of additively manufactured materials in the cloud-based bisque infrastructure, Integr. Mater. Manuf. Innov. 8 (1) (2019) 37–51.
[90] Mohammadreza Yaghoobi, Sriram Ganesan, Srihari Sundar, Aaditya Lakshmanan, Shiva Rudraraju, John E. Allison, Veera Sundararaghavan, Prisms-plasticity: an open-source crystal plasticity finite element software, Comput. Mater. Sci. 169 (2019) 109078.
[91] Mohammadreza Yaghoobi, Krzysztof S. Stopka, Aaditya Lakshmanan, Veera Sundararaghavan, John E. Allison, David L. McDowell, Prisms-fatigue computational framework for fatigue analysis in polycrystalline metals and alloys, npj Comput. Mater. 7 (1) (2021) 1–12.
[92] Romain Quey, Matthew Kasemer, The neper/fepx project: free / open-source polycrystal generation, deformation simulation, and post-processing, IOP Conf. Ser., Mater. Sci. Eng. 1249 (1) (jul 2022) 012021, https://doi.org/10.1088/1757-899X/1249/1/012021, https://dx.doi.org/10.1088/1757-899X/1249/1/012021.
[93] Clement Ribart, Aldo Marano, Henry Proudhon, Multimodal analysis of the early stage of plasticity in a polycrystalline titanium sample: EBSD analysis, https://doi.org/10.5281/zenodo.12801865, 2024.
[94] Clement Ribart, Aldo Marano, Henry Proudhon, Multimodal Analysis of the Early Stage of Plasticity in a Polycrystalline Titanium Sample: DCT to CPFFT, July 2024.
[95] Clement Ribart, Aldo Marano, Henry Proudhon, Multimodal analysis of the early stage of plasticity in a polycrystalline titanium sample: CPFFT simulation, https://doi.org/10.5281/zenodo.12802322, July 2024.
[96] J. Besson, R. Foerch, Large scale object-oriented finite element code design, Comput. Methods Appl. Mech. Eng. (ISSN 0045-7825) 142 (1–2) (1997) 165–187, https://doi.org/10.1016/S0045-7825(96)01124-3.
[97] Romain Quey, Loïc Renversade, Optimal polyhedral description of 3d polycrystals: method and application to statistical and synchrotron x-ray diffraction data, Comput. Methods Appl. Mech. Eng. (ISSN 0045-7825) 330 (2018) 308–333, https://doi.org/10.1016/j.cma.2017.10.029.
[98] F. Bachmann, H. Bale, N. Gueninchault, C. Holzner, E.M. Lauridsen, 3D grain reconstruction from laboratory diffraction contrast tomography Xnovo, J. Appl. Crystallogr. (ISSN 1600-5767) 52 (3) (June 2019) 643–651, https://doi.org/10.1107/S1600576719005442.
[99] F. NGuyen, T. Kanit, F. Maisonneuve, A. Imad, Efficient boundary surface reconstruction from multi-label volumetric data with mathematical morphology, Comput. Graph. (ISSN 0097-8493) (2023), https://doi.org/10.1016/j.cag.2023.10.003, https://www.sciencedirect.com/science/article/pii/S0097849323002406.
[100] Boyer, Collings, Welsch, Materials Properties Handbook: Titanium Alloys - ASM International, ASM, Materials Park, USA, ISBN 978-0-87170-481-8, 1994.

[101] Wolfgang Ludwig, P. Reischig, Andrew King, Michael Herbig, E.M. Laurdisen, G.N. Johnson, J. Marrow, Jean-Yves Buffiere, Three-dimensional grain mapping by X-ray diffraction contrast tomography and the use of Friedel pairs in diffraction data analysis, Rev. Sci. Instrum. 80 (3) (2009) 033905, https://doi.org/10.1063/1.3100200.

[102] H.F. Poulsen, S.F. Nielsen, E.M. Lauridsen, S. Schmidt, R.M. Suter, U. Lienert, L. Margulies, T. Lorentzen, D. Juul Jensen, Three-dimensional maps of grain boundaries and the stress state of individual grains in polycrystals and powders, J. Appl. Crystallogr. 34 (6) (Dec 2001) 751–756, https://doi.org/10.1107/S0021889801014273.

[103] Péter Reischig, Andrew King, Laura Nervo, Nicola Viganò, Yoann Guilhem, Willem Jan Palenstijn, K. Joost Batenburg, Michael Preuss, Wolfgang Ludwig, Advances in X-ray diffraction contrast tomography: flexibility in the setup geometry and application to multiphase materials, J. Appl. Crystallogr. 46 (2) (2013) 297–311, https://doi.org/10.1107/S0021889813002604.

[104] N. Vigano, W. Ludwig, K.J. Batenburg, Reconstruction of local orientation in grains using a discrete representation of orientation space, J. Appl. Crystallogr. 47 (6) (2014) 1826–1840, https://doi.org/10.1107/S1600576714020147.

[105] Henry Proudhon, Thiebaud Richeton, Damien Texier, Ayyoub Dziri, Quentin Sirvin, Marc Legros, Correlative Analysis of EBSD and High Speed Nanoindentation Mapping Datasets in Pure Titanium, March 2024.

[106] Aldo Marano, Lionel Gélébart, Samuel Forest, Intragranular localization induced by softening crystal plasticity: analysis of slip and kink bands localization modes from high resolution fft-simulations results, Acta Mater. 175 (2019) 262–275.

[107] Arina Marchenko, Matthieu Maziere, Samuel Forest, Jean-Loup Strudel, Crystal plasticity simulation of strain aging phenomena in α-titanium at room temperature, Int. J. Plast. 85 (2016) 1–33.

[108] Hans Conrad, Effect of interstitial solutes on the strength and ductility of titanium, Prog. Mater. Sci. (ISSN 0079-6425) 26 (2) (January 1981) 123–403, https://doi.org/10.1016/0079-6425(81)90001-3.

[109] E.A. Anderson, D.C. Jillson, S.R. Dunbar, Deformation mechanisms in alpha titanium, Trans. AIME 197 (1953), https://www.scopus.com/inward/record.uri?eid=2-s2.0-0039393269&partnerID=40&md5=3644d0069c293e7ae23090573cbb14a9, Cited by: 44.

[110] V. Gerold, H.P. Karnthaler, On the origin of planar slip in fcc alloys, Acta Metall. 37 (8) (1989) 2177–2183.

[111] D. Lunt, T. Busolo, X. Xu, J. Quinta Da Fonseca, M. Preuss, Effect of nanoscale $\alpha 2$ precipitation on strain localisation in a two-phase ti-alloy, Acta Mater. 129 (2017) 72–82.

[112] A.D. Kammers, S. Daly, Digital image correlation under scanning electron microscopy: methodology and validation, Exp. Mech. (ISSN 0014-4851) 53 (9) (November 2013) 1743–1761, https://doi.org/10.1007/s11340-013-9782-x, 1741–2765.

[113] Yanis Balit, Eric Charkaluk, Andrei Constantinescu, Digital image correlation for microstructural analysis of deformation pattern in additively manufactured 316L thin walls, Addit. Manuf. (ISSN 2214-8604) 31 (January 2020) 100862, https://doi.org/10.1016/j.addma.2019.100862.

[114] J.-C. Stinville, M.-A. Charpagne, R. Maaß, H. Proudhon, W. Ludwig, P.G. Callahan, F. Wang, I.J. Beyerlein, M.P. Echlin, T.M. Pollock, Insights into plastic localization by crystallographic slip from emerging experimental and numerical approaches, Annu. Rev. Mater. Res. (ISSN 1531-7331) 53 (1) (2023) 275–317, https://doi.org/10.1146/annurev-matsci-080921-102621.

[115] D. Shechtman, D.G. Brandon, Orientation dependent slip in polycrystalline titanium, J. Mater. Sci. (ISSN 1573-4803) 8 (9) (September 1973) 1233–1237, https://doi.org/10.1007/BF00549337.

[116] J.F. Nye, Some geometrical relations in dislocated crystals, Acta Metall. (ISSN 0001-6160) 1 (2) (March 1953) 153–162, https://doi.org/10.1016/0001-6160(53)90054-6.

[117] Ekkehart Kröner, Allgemeine Kontinuumstheorie der Versetzungen und Eigenspannungen, Arch. Ration. Mech. Anal. (ISSN 1432-0673) 4 (1) (January 1959) 273–334, https://doi.org/10.1007/BF00281393.

[118] Paolo Cermelli, Morton E. Gurtin, On the characterization of geometrically necessary dislocations in finite plasticity, J. Mech. Phys. Solids (ISSN 0022-5096) 49 (7) (July 2001) 1539–1568, https://doi.org/10.1016/S0022-5096(00)00084-3.

[119] Y. Guo, D.M. Collins, E. Tarleton, F. Hofmann, A.J. Wilkinson, T.B. Britton, Dislocation density distribution at slip band-grain boundary intersections, Acta Mater. 182 (2020) 172–183, https://doi.org/10.1016/j.actamat.2019.10.031.

[120] Wyatt A. Witzen, Andrew T. Polonsky, Paul F. Rottmann, Kira M. Pusch, McLean P. Echlin, Tresa M. Pollock, Irene J. Beyerlein, Boundary characterization using 3D mapping of geometrically necessary dislocations in AM Ta microstructure, J. Mater. Sci. (ISSN 1573-4803) 57 (21) (June 2022) 9885–9902, https://doi.org/10.1007/s10853-022-07074-2.

[121] T. Vermeij, R.H.J. Peerlings, M.G.D. Geers, J.P.M. Hoefnagels, Automated identification of slip system activity fields from digital image correlation data, Acta Mater. (ISSN 1359-6454) 243 (2023) 118502, https://doi.org/10.1016/j.actamat.2022.118502.

[122] Hugh Simons, Anders Clemen Jakobsen, Sonja Rosenlund Ahl, Carsten Detlefs, Henning Friis Poulsen, Multiscale 3D characterization with dark-field x-ray microscopy, Mater. Res. Soc. Bull. 41 (6) (2016) 454–459, https://doi.org/10.1557/mrs.2016.114.

[123] Aldo Marano, Clement Ribart, Henry Proudhon, Multimodal data set for the investigation of the early stage of plasticity in a polycrystalline titanium sample, https://doi.org/10.5281/zenodo.11091756, April 2024.

[124] D. Rowenhorst, A.D. Rollett, G.S. Rohrer, M. Groeber, M. Jackson, P.J. Konijnenberg, M. De Graef, Consistent representations of and conversions between 3D rotations, Model. Simul. Mater. Sci. Eng. (ISSN 0965-0393) 23 (8) (Dec 2015) 083501, https://doi.org/10.1088/0965-0393/23/8/083501.

[125] Jean Christophe Glez, Julian Driver, Orientation distribution analysis in deformed grains, J. Appl. Crystallogr. 34 (3) (Jun 2001) 280–288, https://doi.org/10.1107/S0021889801003077.